Article:
Asteris, PG, Lemonis, ME, Le, T-T et al. (1 more author) (2021) Evaluation of the Ultimate Eccentric Load of Rectangular CFSTs using Advanced Neural Network Modeling. Engineering Structures, 248. 113297. ISSN 0141-0296

https://doi.org/10.1016/j.engstruct.2021.113297

Evaluation of the ultimate eccentric load of rectangular CFSTs using advanced neural network modeling

Panagiotis G. Asteris[1*], Minas E. Lemonis[1], Tien-Thinh Le[2,3] and Konstantinos Daniel Tsavdaridis[4]

[1] *Computational Mechanics Laboratory, School of Pedagogical and Technological Education, Heraklion, GR 14121, Athens, Greece*

[2] *Faculty of Mechanical Engineering and Mechatronics, PHENIKAA University, Yen Nghia, Ha Dong, Hanoi 12116, Viet Nam. Email: thinh.letien@phenikaa-uni.edu.vn*

[3] *PHENIKAA Research and Technology Institute (PRATI), A&A Green Phoenix Group JSC, No.167 Hoang Ngan, Trung Hoa, Cau Giay, Hanoi 11313, Viet Nam*

[4] *School of Civil Engineering, Faculty of Engineering and Physical Sciences, University of Leeds, Woodhouse Lane, LS2 9JT Leeds, UK*

[*] *Corresponding author, Professor, E-mail: asteris@aspete.gr; panagiotisasteris@gmail.com*

Abstract:

In this paper an Artificial Neural Network (ANN) model is developed for the prediction of the ultimate compressive load of rectangular Concrete Filled Steel Tube (CFST) columns, taking into account load eccentricity. To this end, an experimental database of CFST specimens from the literature has been compiled, totaling 1224 individual tests, both under concentric and under eccentric loading. Except for eccentricity, other parameters taken into consideration include the cross section width, height and thickness, the steel yield limit, the concrete strength and the column length. Both short and long specimens were evaluated. The architecture of the proposed ANN model was optimally selected, according to predefined performance metrics. The developed model was then compared against available design codes. It was found that its accuracy was significantly improved while maintaining a stable numerical behavior. The explicit equation that describes mathematically the ANN is offered in the paper, for easier implementation and evaluation purposes.

***Keywords*:** Concrete-Filled Steel Tube (CFST); artificial neural networks (ANNs); load eccentricity; rectangular CFST; ultimate load

Nomenclature

ANN(s)	Artificial Neural Network(s)
A_c	Area of Concrete Core Section
A_s	Area of Steel Tube Section
A_{sc}	Area of Composite Section
B	Width of Tubes Section
BPNN	Back Propagation Neural Network
CFST	Concrete Filled Steel Tube
Co	Competitive transfer function
E_c	Concrete Modulus of Elasticity
E_s	Steel Modulus of Elasticity
f'_c	Concrete Compressive Strength
f_y	Steel Yield Strength
f_u	Steel Ultimate Strength
GUI	Graphical User Interface
H	Height of Tubes Section
HTS	Hyperbolic Tangent Sigmoid transfer function
I_s	Moment of Inertia of Steel Tube Section
I_c	Moment of Inertia of Concete Core Section
L	Length of Column
L_e	Effective Length of Column
Li	Linear transfer function
LS	Log-Sigmoid transfer function
MAPE	Mean Absolute Percentage Error
MSE	Mean Square Error
N	Axial Load Capacity
N_b	Buckling Capacity of Column
N_{cr}	Elastic Critical Bucking Load
N_{pl}	Squash Load
NRB	Normalized Radial Basis transfer function
PLi	Positive Linear transfer function
R	Pearson correlation coefficient
RB	Radial Basis transfer function
SM	Soft Max transfer function
SSE	Sum Square Error
SP	Superplasticizer
SSL	Symmetric Saturating Linear transfer function
t	Wall Thickness of Steel Tubes
TB	Triangular Basis transfer function
ξ	Confinement Factor
ρ	Concrete Density

1. Introduction

Reinforced concrete and bare steel columns are well known and widely used in building construction, enjoying a thorough experimental verification of their behavior, established standards for their design, and a manufacturing and detailing expertise readily available in the industry. Each one, offers a number of advantages but is also accompanied by a number of restrictions. Specifically, bare steel columns offer great strength, with a minimal footprint and also facilitate construction speed. However, they often require lateral restraining in order to prevent instabilities such as flexural buckling or flexural-tortional buckling. On the other hand, reinforced concrete columns, offer satisfactory strength, generally unaffected by instabilities, however this is limited by the level of confinement available to concrete while their footprint on floor space is increased and speed of construction is slower.

Concrete Filled Steel Tube (CFST) columns offer a combination of the advantages originating from their concrete and steel parts. They are constructed from a steel tube, most commonly of circular or rectangular section, which is filled with concrete. Normally, no steel reinforcement is placed within the concrete. The required confinement for the concrete is provided by the steel tube, surrounding the concrete core. Furthermore, the steel tube serves as formwork for the concrete, enhancing speed of construction. On the other hand, the concrete core restraints inward deformations of the steel tube, enhancing its local stability, whereas the combined stiffness of steel and concrete parts, enhances the column global stability. These synergies, lead to increased strength characteristics, surpassing that of the respective individual parts.

This paper investigates the ultimate load capacity of rectangular CFSTs taking into account load eccentricity. Considering the axial compressive capacity, a great number of experimental investigations is available in the literature, most often for square but also for non-square rectangular sections. Significant early works include Kloppel & Goder (1957)[1], Furlong (1967)[2], Knowles and Park (1969)[3], Gardner and Jacobson (1967)[4] and Tomii et al. (1977)[5]. Key aspects of rectangular CFST design that influence their ultimate behavior have become the subject of research investigation over the past years. These include the slenderness of the steel section, the length of the column, the aspect ratio of the tube section dimensions, the use of high strength steel or concrete and the detailing. The slenderness of the steel section, typically expressed by a width to thickness ratio B/t, affects the local stability of the tube. It has been experimentally investigated by Uy (1998)[6], Sakino et al. (2004)[7], Chitawadagi et al (2010)[8], Evirgen et al. (2014)[9], Chen et al. (2018)[10]. Higher values of the B/t ratio have been reported to cause premature local buckling phenomena that lead to loss of concrete confinement, limiting the ultimate load capacity. Regarding the length of a column CFST member, most of the experimental investigations focus on short specimens. Testing of long specimens however, allows potential global buckling phenomena to emerge and affect load capacity. Such tests have been conducted by Han and Yao (2003)[11], Mursi and Uy (2004)[12], Lue et al. (2007)[13], Yu et al. (2008)[14], Dundu (2016)[15], Khan et al. (2017)[16]. The aspect ratio of the steel tube dimensions, influences the confinement conditions in the concrete core and therefore has an impact on the final axial load capacity. Relevant investigations, available by Gardner and Jacobson (1967)[4], Han (2002)[17], Liu et al (2003)[18], Liu (2005)[19], Du et al.

(2016)[20], Ibanez et al. (2018)[21] indicate that square sections provide better concrete confinement whereas higher aspect ratios lead to deteriorated strength and ductility.

In actual conditions, CFST columns are expected to carry not only axial loads but also bending moments. However, the evaluation of the ultimate load carrying capacity under such conditions, has attracted less research efforts, compared to purely axial loading. Initial test results are available in Knowles & Park (1969)[3], Bridge (1976)[22] and Khalil & Zeghiche(1989)[23]. More extensive programmes were presented by Cederwa et al. (1990)[24] and Khalil & Al-Rawdan (1996)[25] who both evaluated the influence of load eccentricity, along with varying values of steel and concrete strength. Also, Matsui & Tsuda (1996)[26] investigated experimentally square CFSTs under varying eccentricity ratios and member lengths, covering both short and long columns. An extensive parametric testing of eccentrically loaded square CFSTs has been presented by Nakahara & Sakino (2000)[27], including specimens with high strength concrete and high strength steel. Uy (2000)[28], investigated the local buckling response of eccentrically loaded thin walled CFSTs, while Mursi and Uy (2003)[29] extended the scope to the interaction of local and global buckling phenomena and Mursi and Uy (2004)[30] to high strength steel. Zhang et al. (2004)[31] presented experiments on square CFSTs, parametrically investigating, eccentricity ratio, steel to concrete ratio and member length. Liu (2004) [32], presented experimental testing on rectangular CFSTs under eccentric loading, using high strength steel and varying parameters the cross section aspect ratio, the eccentricity ratio and member slenderness. Also Liu (2006) [33], furtherly tested eccentrically loaded rectangular CFSTs, including short and long ones, evaluating different cross section aspect ratios and eccentricity ratios, as well. Varma et al. (2002)[34], tested square CFSTs under constant axial loading and monotonically increasing flexure. The parameters of the study included the steel section width to thickness ratio, the steel yield limit and the axial load. In addition, Varma et al. (2004)[35] extended the scope of testing to cyclically imposed flexure. Fujimoto et al. (2004)[36], reported the results of an extended testing program on eccentrically loaded high strength CFSTs. Under examination were the shape of the cross-section, including rectangular ones, the steel section slenderness and material strengths. Zhang and Guo (2007)[37], presented an extended study on eccentrically loaded rectangular CFSTs, using high strength concrete and varying member slenderness, cross section aspect ratio, steel to concrete ratio and eccentricity. On the other hand, Qu et al. (2013)[38], investigated the behavior of rectangular CFSTs under combined axial and uniaxial or biaxial bending, evaluating against varying concrete and steel strength, eccentricity and cross section aspect ratio. Lee et al. (2016)[39] investigated thin walled rectangular CFSTs, using high strength steel and varying the steel strength, the cross-section slenderness and the load eccentricity. Du et al. (2017) [40] investigated the behavior of rectangular CFSTs under eccentric compressive loading, employing varying values of eccentricity ratio, concrete strength, tube section aspect ratio and width to thickness ratio. Also, high strength square CFSTs were tested by Li et al. (2018)[41], investigating their behavior for different steel to concrete ratios and eccentricity ratios.

Methodologies for the estimation of the capacity of CFSTs under eccentric loading are also available in the literature. Mursi and Uy (2003)[29] developed a numerical model, that takes into account load eccentricity along with local and global buckling phenomena. The model was capable to produce the entire load vs. deflection curve, inducing post-critical region. Similarly,

Zhang et al. (2004)[31] developed a nonlinear program, for the calculation of the load vs. deflection curve of CFSTs under eccentric load. Liu (2006) [33] and Zhang and Guo (2007)[37], also proposed a numerical models for the load vs. deflection curve of high strength CFSTs, assuming global buckling conditions. Patel et al. (2012a[42] and 2012b[43]), developed a numerical methodology, employing fiber based elements, for the prediction of entire load vs deflection curve of thin walled rectangular CFSTs. The methodology can simulate local and global buckling phenomena and accounts for load eccentricity too. Du et al. (2017) [40] proposed M-N interaction curves, based on an analytical methodology, for rectangular, high strength CFSTs under combined axial force and bending moment. Similarly, Li et al. (2018) calibrated an analytical methodology for the estimation of M-N interaction curves for rectangular, high strength CFSTs. Recently, Patel (2020)[44] extended fiber based numerical discretization methodology for the modeling of rectangular CFST beam-columns with rounded edges.

The use of soft computing techniques for the prediction of ultimate load of CFSTs is a topic with an emerging number of research efforts. Güneyisi et al. (2016)[45], developed a model for the estimation of the ultimate load of circular CFSTs, employing a gene expression programming technique. The model was calibrated through a database of 314 experimental tests. Du et al. (2017) [46] developed an ANN to predict the axial capacity of rectangular CFST, using as input parameters sectional depth, width, thickness, and the strengths of steel and concrete materials. A database of 305 experimental specimens was utilized for its training and validation. Jayalekshmi et al. (2018) [47] employing a trained ANN model they developed, validated an empirical formulation for the estimation of the axial strength of circular CFSTs. Tran et al. (2019) [48] developed an ANN model for the prediction of the ultimate axial load of square CFSTs, using a database of 300 experimental specimens. Utilizing the ANN model as reference, they also validated an empirical formula for same problem. Ren et al. (2019) [49], predicted the ultimate load of square CFSTs using a hybrid algorithm based on a support vector machine, with parameters optimized using a particle swarm optimization technique. The model was calibrated using an experimental database, consisting of 180 specimens and accounted as inputs material properties (steel and concrete strength and modulus of elasticity) along with tube width, thickness and column length. Le and Phan (2020) [50], developed a model for the ultimate load of rectangular CFST columns, employing an adaptive neurofuzzy inference system. The model included as inputs the steel and concrete strengths and the tube dimensions, namely depth, width, thickness, with column length as well. Zarringol et al. (2020) [51] developed an ANN model for the ultimate concentric or eccentric load of rectangular and circular CFSTs. For the training of the model, four different groups of experimental specimens were employed for each particular case, resulting in four different sets of weights and biases. Empirical equations were also given, based on the mathematical formulations of the developed ANNs. Javed et al. (2020) [52] employed gene expression programming in order to predict the axial capacity of circular CFST long columns. An experimental database of 227 specimens was used for the development of the model. Recently, Asteris et al. (2021)[54] developed a hybrid ANN model, incorporating a Balancing Motion Composite Optimization technique for the estimation of the ultimate load of rectangular CFST columns. A database of 422 experimental specimens was used for the development and validation of the model. Naser et al. (2021)[53] implemented both genetic programming and gene expression programming, in order to predict the axial concentric or eccentric ultimate load of rectangular and circular CFST columns. A database of a total 3103

experimental specimens, splitted to four groups, in order to cover particular cases. Also, Le et al. (2021)[55], predicted the ultimate concentric load of square and rectangular CFSTs using an ANN, trained and validated through an experimental database of 880 specimens.

2. Research Significance

This work attempts to develop an ANN model for the prediction of the ultimate capacity of rectangular CFSTs under eccentric compressive load. Such a loading is much more interesting from a design perspective, since an interaction of axial force and bending moment is commonly encountered in the columns of frame structures. Similarly, the adoption of rectangular CFST sections is often preferable considering architectural requirements, while it allows for the design of CFSTs with different strengths around each axis, so that they are better fitted to the demands of the structure.

While there are many research works regarding concentric axial loading, along with explicit analytical methodologies for the estimation of the load carrying capacity, the same cannot be told in the case of eccentric loading or combined compression and flexure in general. The experimental works, while growing in numbers, are considerably less. As a result, a thorough understanding regarding the influence of such a loading interaction on the failure mechanisms requires additional research. The available design methodologies, currently limit their field of application, in regard to material strengths and cross section slenderness. Therefore, some potential benefits from the use of CFSTs are hindered. Specifically, the increased stiffness of CFSTs compared to bare steel sections, facilitates the use of more slender steel tubes. Also, with the use of high strength concrete and steel, the required cross section and the footprint on floor space could be reduced. Therefore, a broader field of application is wanted that covers the space between available experimental results. The ANN technique adopted herein, possesses the capability to optimally interpolate between the poly-parametric space of relevant experimental data. Furthermore, the resulting ANN model, typically is quite simple to implement programmatically and very efficient computationally. To the contrary, typical design code implementations require iterations in order to determine the equilibrium of internal forces in the cross-section or to solve implicit equations between the parameters of the problem. Furthermore, the accuracy of an ANN can be easily enhanced, once more experimental works become available.

3. Design codes for eccentrically loaded CFSTs

In this section a presentation of existing methodologies in design codes, for the estimation of the compressive load of CFSTs, accounting for load eccentricity is made. The analysis covers the case of single eccentricity so that conditions of constant bending moment around a single axis apply. Also, the application of safety factors is not included in the presentation in this section, so that a comparison between different codes becomes more objective. Specifically, the proposals from the European code EN1994 [45], the American code AISC360-16 [57], the Japanese AIJ [58], and the Australian/New Zealand AS/NZS 2327:2017 [59] is included. All of these methodologies place limits on their field of application, restricting their use outside them. Most commonly the limits are related to steel and concrete material strength and the steel section slenderness. Table 1 summarizes these

limits for all examined analytical methodologies.

Table 1. Field of application of various code standards for the design of CFST columns

Code	f_y (MPa)	$f_c^{'}$, (MPa)	Section slenderness	Other
EN1994 [45]	$235 \le f_y \le 460$	$25 \le f_c' \le 50$	$\frac{H}{t} \le 52\sqrt{\frac{235}{f_y}}$	$0.2 \le \delta \le 0.9$ $\begin{cases}\delta = \frac{A_s f_y}{N_{pl}} \\ N_{pl} \text{ from eq. 1}\end{cases}$
AISC 360-16[57]	$f_y \le 525$	$21 \le f_c' \le 69$	$\frac{H}{t} \le 5\sqrt{\frac{E_s}{f_y}}$	$A_s \ge 0.01 A_{sc}$
AIJ [58]	$235 \le f_y \le 355$	$18 \le f_c' \le 60$	$\frac{H}{t} \le 1.5\frac{735}{\sqrt{\min\{f_y; 0.7f_u\}}}$	$\frac{L_e}{B} \le 50$
AS/NZS 2327 [59]	$f_y \le 690$	$20 \le f_c' \le 100$	$\frac{H}{t}\sqrt{\frac{f_y}{250}} \le 141$	$0.2 \le \delta \le 0.9$ $\begin{cases}\delta = \frac{A_s f_y}{N_{pl}} \\ N_{pl} \text{ from eq. 13}\end{cases}$

*A_{sc}, A_s, and A_c are the areas of the total cross section, the steel tube and the concrete core, respectively

H, B are the height and width of the cross section, respectively, t is the tube wall thickness

L_e is the column effective length

3.1 Eurocode EN1994

Axial compression

Eurocode EN1994[45], provides the following formula for the estimation of the squash load of a CFST column, under axial compression:

$$N_{pl} = f_y A_s + f_c^{'} A_c \quad (1)$$

For long columns, the ultimate load is determined by flexural buckling however. This is taken into account through a reduction factor χ, and as a result the column ultimate axial load is given by:

$$N_u = \chi N_{pl}, \text{ with } \chi \le 1 \quad (2)$$

The estimation of χ is based on the buckling curves, provided by Eurocode EN1993 [60], using a column effective slenderness $\bar{\lambda} = \sqrt{N_{pl}/N_{cr}}$, where N_{cr} is the critical buckling load. The latter is found employing a combined flexural rigidity $(EI)_{eff}$ equal to:

$$(EI)_{eff} = E_s I_s + 0.6 E_c I_c \quad (3)$$

where, I_s, I_c are the moments of inertia of the steel section and the concrete core, respectively and E_s, E_c the moduli of elasticity for the same components.

Flexure

In the absence of any axial load, the flexural resistance of an CFST is determined by the full plastic moment of its composite section M_{pl}. Figure **1**b illustrates the assumption for internal stresses proposed by EN1994[45]. The concrete compressive block is assumed having a uniform f_c' stress, in the case of filled members.

Combined axial compression and flexure

For the resistance of a CFST member under combined axial compression and single axis bending, EN1994[45], proposes a modified moment strength due to interaction. The following expression is provided:

$$M_N = a_M \mu M_{pl} \tag{4}$$

where a_M is 0.9 of steel grades up to S355 inclusive, and 0.8 for higher grades, M_{pl} is the plastic bending resistance without axial load and μ the interaction factor. The calculation of μ is facilitated by an interaction M-N diagram, as shown in Figure **1**a, assuming plastic conditions throughout the composite section. Except for the interaction curve, which is constructed from all possible M,N pairs, a simplified curve is also provided, which is constructed from four key M,N pairs. In the case of load eccentricity, the flexure is constant along the column length, with a moment $M = N\ e$. Thus, the ultimate axial force, on the basis of EN1994, can be determined from equation 4 as:

$$N_{u,e} = a_M \mu \frac{M_{pl}}{e} \tag{5}$$

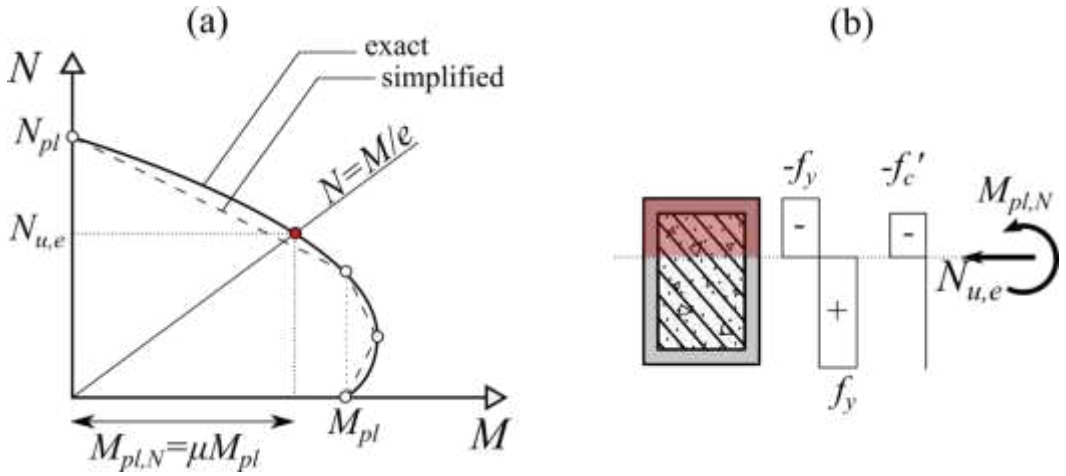

Figure 1. M-N interaction diagram according to EN1994[45] (a) and internal plastic stress distribution in the composite section, under combined axial compression and flexure (b)

3.2 AISC 360-16

Axial compression

Depending on the slenderness of the column member, American standard AISC360-16 [57], provides the following two cases for the calculation of the CFST axial compressive capacity:

$$N_u = \begin{cases} N_{no}\left(0.658^{\left(\frac{N_{no}}{N_{cr}}\right)}\right) & \text{, if } \dfrac{N_{no}}{N_{cr}} \le 2.25 \\ 0.877 N_{cr} & \text{, if } \dfrac{N_{no}}{N_{cr}} > 2.25 \end{cases}, \tag{6}$$

where N_{cr} is the elastic critical buckling load of the column, which is calculated using an effective flexural rigidity $(EI)_{eff} = E_s I_s + C_3 E_c I_c$ and N_{no} provides the strength of the composite section, taking into account local buckling phenomena, using the following equation:

$$N_{no} = \begin{cases} N_{pl} & , \text{if } \lambda < \lambda_p \\ N_{pl} - (N_{pl} - N_y)\dfrac{(\lambda - \lambda_p)^2}{(\lambda_r - \lambda_p)^2} & , \text{if } \lambda_p \leq \lambda < \lambda_r \\ f_{cr} A_s + 0.7 f_c' A_c & , \text{if } \lambda \geq \lambda_r \end{cases} \quad (7)$$

In the last expression, N_{pl} and N_y provide the plastic and yield load, respectively of the composite section, f_{cr} is the critical stress for the steel section local buckling, whereas λ describes the slenderness of the steel section and parameters λ_p, λ_p are classification limits. All these, along with parameter C_3 and the concrete modulus of elasticity E_c, required for the effective flexural rigidity, can be obtained by following the expressions:

$$\begin{cases} N_{pl} = f_y A_s + 0.85 f_c' A_c \\ N_y = f_y A_s + 0.7 f_c' A_c \\ f_{cr} = 9 E_s A_s / \lambda^2 \\ \lambda = (H - 2t)/t \\ \lambda_p = 2.26\sqrt{E_s / f_y} \\ \lambda_r = 3.00\sqrt{E_s / f_y} \\ C_3 = 0.45 + \dfrac{3A_c}{A_{sc}} \leq 0.9 \\ E_c = 0.043 \rho^{1.5} \sqrt{f_c'} \end{cases} \quad (8)$$

where ρ is the density of concrete in kg/m^3 and the resulting E_c is given in MPa.

Flexure

Depending on the steel section resistance to local buckling, three cases are distinguished for the flexural strength of a CFST, according to AISC360-16 [57]:

$$M_u = \begin{cases} M_p & , \text{if compact} \\ M_p - (M_p - M_y)\dfrac{\lambda - \lambda_p}{\lambda_r - \lambda_p} & , \text{if non-compact} \\ M_{cr} & , \text{if slender} \end{cases} \quad (9)$$

where M_p is the full plastic moment strength of the cross section, assuming a compressive stress limit for concrete equal to $0.85 f_c'$, M_y is the yield moment of the cross-section, corresponding to yielding of the tension flange and first yield of the compression flange with concrete compressive block limited to $0.7 f_c'$ stress, and M_{cr} is the first yield moment which corresponds to first yielding of the tension flange while the compression

flange is limited to critical stress f_{cr} (see eq. 8) and the concrete block is limited to $0.7f_c'$ stress. Figure **2** illustrates the three different cases.

Combined axial compression and flexure

When there is interaction of axial compression and flexure, as happens in an eccentrically loaded CFST column, AISC360-16 [57] provides two alternative M-N interaction diagrams. The first one is described by the following expressions:

$$\begin{cases} \dfrac{N}{N_u} + \dfrac{8}{9}\dfrac{M}{M_u} = 1 & \text{, if } \dfrac{N}{N_u} \geq 0.2 \\ \dfrac{N}{2N_u} + \dfrac{M}{M_u} = 1 & \text{, if } \dfrac{N}{N_u} < 0.2 \end{cases} \tag{10}$$

where N_u and M_u the respective capacities of the composite section to axial compression and flexure, as described previously.

The second interaction formula, provided by AISC360-16 [57], is described by the following expressions:

$$\begin{cases} \dfrac{N}{N_u} + \dfrac{1-c_p}{c_m}\dfrac{M}{M_u} = 1 & \text{, if } \dfrac{N}{N_u} \geq c_p \\ \dfrac{1-c_m}{c_p}\dfrac{N}{N_u} + \dfrac{M}{M_u} = 1 & \text{, if } \dfrac{N}{N_u} < c_p \end{cases} \tag{11}$$

where parameters c_p and c_m depend on the steel to concrete strength ratio $c_{sr} = A_s f_y / A_c f_c'$, and are given by the equations:

$$\begin{cases} c_p = 0.17/c_{sr}^{0.4} & \\ c_m = 1.06/c_{sr}^{0.11} \geq 1 & \text{, if } c_{sr} \geq 0.5 \\ c_m = 0.90/c_{sr}^{0.36} \leq 1.67 & \text{, if } c_{sr} < 0.5 \end{cases} \tag{12}$$

Figure **2**a illustrates the two M-N interaction diagrams, that are produced by equations 10 and 11.

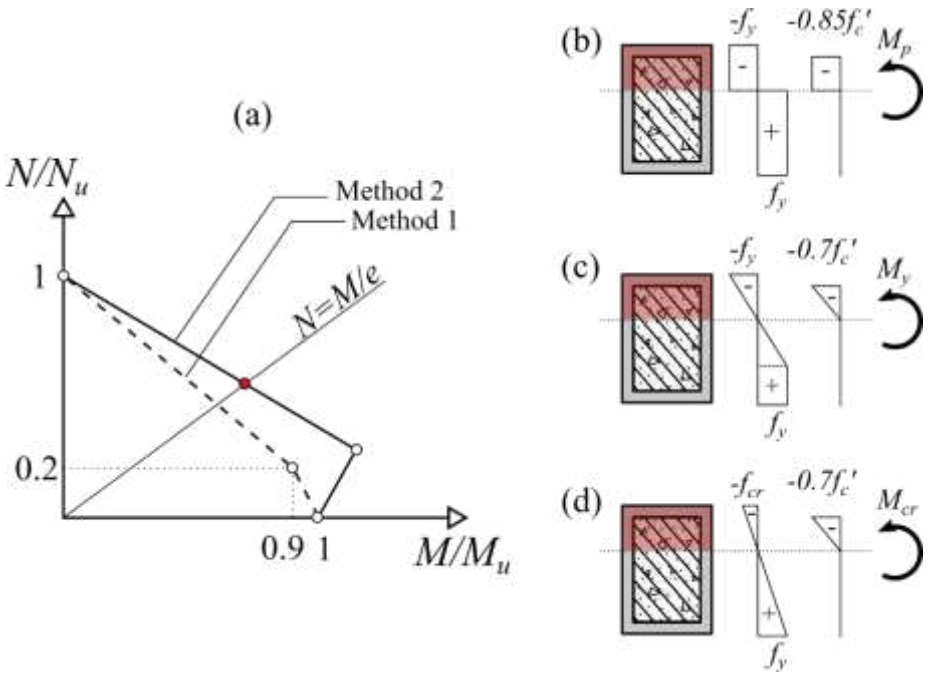

Figure 2. M-N interaction diagrams according to AISC360-16[57] (a) and stress distributions for plastic moment (b), yield moment (c) and the first yield moment.

3.3 AS/NZS 2327: 2017

Axial compression

According to the Australian code AS/NZS 2327:2017[59], the squash load of CFST sections under axial compression is found by the combined resistances of the steel and concrete parts. Ignoring safety factors:

$$N_{pl} = k_f f_y A_s + f_c' A_c, \tag{13}$$

where $k_f = A_e/A_s$ a form factor depending on effective tube area A_e, which accounts for section slenderness. For long columns, flexural buckling is accounted for through a reduction factor a_c, so that the final column capacity is found as:

$$N_u = a_c N_{pl}, \tag{14}$$

with:

$$a_c = \xi \left[1 - \sqrt{1 - \left(\frac{90}{\xi \lambda} \right)^2} \right] \leq 1 \tag{13}$$

where factors λ and ξ depend on column slenderness, imperfections and residual stresses, using the following equations:

$$\lambda = \lambda_\eta + a_a a_b$$
$$\xi = \frac{(\lambda/90)^2 + 1 + \eta}{2(\lambda/90)^2}$$
$$\lambda_\eta = 90\lambda_r$$
$$\lambda_r = \sqrt{N_{pl}/N_{cr}} \quad (15)$$
$$a_a = \frac{2100(\lambda_\eta - 13.5)}{{\lambda_\eta}^2 - 15.3\lambda_\eta + 2050}$$
$$\eta = 0.00326(\lambda - 13.5) \geq 0$$

For the above equations, the critical buckling load of the column N_{cr} is based on an effective flexural rigidity equal to: $E_s I_s + E_c I_c$, where E_c the concrete modulus of elasticity, is reduced if necessary, to account for long term effects. Factor η describes geometrical imperfections, whereas factor a_b accounts for residual stresses, taking values 0 or -0.5 for tubular slender or non-slender (i.e. with $k_f = 1$) sections, respectively

Combined axial compression and flexure

According to AS/NZS 2327:2017[59], the capacity of a CFST under combined compression and bending, is determined assuming rectangular stress blocks (full plastification) for both the steel and the concrete parts of the cross-section, similar to EN1994[45] (see Figure 1). Ignoring safety factors, the maximum compressive stress for concrete is $f_c^{'}$ while the maximum stress for steel is f_y. The ultimate flexural capacity is reduced by a 0.9 factor. From the interaction diagram that is produced for all possible M, N pairs, and taking into account that for eccentric load conditions it is $M = N\ e$, the ultimate compressive load can be determined:

$$N_u = 0.9\frac{M_N}{e} \quad (16)$$

where, M_N is the bending moment capacity of the cross-section accounting for the interaction with the axial force.

3.4 AIJ

Axial compression

The ultimate axial compressive load of square CFST columns according to Japanese code AIJ[58] is found through the following three expressions, accounting for the member slenderness:

$$N_u^{AIJ} = \begin{cases} A_s f_y + 0.85 A_c f_c^{'} \quad (= N_{pl}) & \text{, if: } L_e/B \leq 4 \\ N_{pl} - 0.125(N_{pl} - N_b)\left(\frac{L_e}{B} - 4\right) & \text{, if: } 4 < L_e/B \leq 12 \\ N_b^c + N_b^s \quad (= N_b) & \text{, if: } L_e/B > 12 \end{cases} \quad (17)$$

where, B is the section width, L_e the effective column length and N_b^c, N_b^s, the buckling capacities of the concrete and steel parts of the section, respectively. The first equation represents the squash load of the composite section, while the third one covers failure due to flexural buckling. Buckling capacity of the concrete core is estimated through the expression:

$$N_b^c = \begin{cases} \frac{2}{1+\sqrt{\bar{\lambda}_c^4+1}} 0.85 A_c f_c^{'} & , \text{ if: } \bar{\lambda}_c \le 1 \\ 0.83 e^{[C_c(1-\bar{\lambda}_c)]} 0.85 A_c f_c^{'} & , \text{ if: } \bar{\lambda}_c > 1 \end{cases} \quad (18)$$

where:

$$\begin{cases} \bar{\lambda}_c = \lambda_c \sqrt{\varepsilon_u^c}/\pi \\ \varepsilon_u^c = 0.00093(0.85 f_c^{'})^{0.25} \\ C_c = 0.568 + 0.00612 f_c^{'} \end{cases} \quad (19)$$

Similarly, buckling capacity of the steel tube is estimated through the expression:

$$N_b^s = \begin{cases} A_s f_y & , \text{ if: } \bar{\lambda}_s < 0.3 \\ \left[1 - 0.545\left(\bar{\lambda}_s - 0.3\right)\right] A_s f_y & , \text{ if: } 0.3 \le \bar{\lambda}_s < 1.3 \\ \frac{1}{1.3} \frac{\pi^2 E_s I_s}{{L_e}^2} & , \text{ if: } \bar{\lambda}_s \ge 1.3 \end{cases} \quad (20)$$

where:

$$\bar{\lambda}_s = \frac{\lambda_s}{\pi} \sqrt{\frac{f_y}{E_s}} \quad (21)$$

In the above expressions, λ_c and λ_c are the slenderness ratios of the concrete and steel parts of the column.

Combined axial compression and flexure

For relatively short CFST columns (i.e. no longer than 12 times the width), the ultimate eccentric compressive load according to AIJ[58] code is given by the following expression:

$$N_u = \bar{x} H_c^2 0.85 f_c + 2(2\bar{x} - 1) H_c t f_y \quad (22)$$

where $H_c = H - 2t$, $\bar{x} = x/H_c$ and x the depth of the compressive area of the cross section. The last equation is defined assuming square cross-section with rectangular stress blocks, with ultimate stress $0.85 f_c'$ for the concrete and f_y for the steel, as shown in Figure **3**

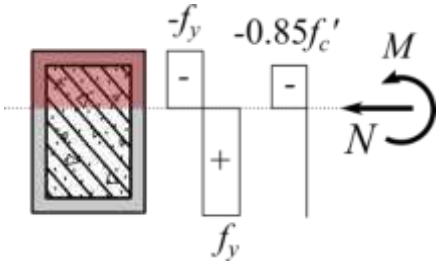

Figure 3. Stress distribution for the plastic load under combined compression and flexure according to AIJ[44].

For more slender columns (i.e., at least 12 times longer than their width), AIJ code suggests an ultimate load based on the superposition of two M-N interaction diagrams, each representing the concrete and the steel part. Taking into account that $M = Ne$, in the case of load eccentricity, the following implicit equations apply:

$$\begin{cases} M_u = N_u e = \dfrac{1}{C_M}\left[M_u^c + M_{pl}^s\left(1 - \dfrac{N_u}{N_k}\right)\right] & \text{, if } N_u \le N_b^c \\ M_u = N_u e = \dfrac{1}{C_M} M_u^s\left(1 - \dfrac{N_b^c}{N_k}\right) & \text{, if } N_u > N_b^c \end{cases} \tag{23}$$

The buckling capacity of the concrete core N_b^c is given by equation 18, N_k is the column Euler load, using a flexural rigidity equal to $0.2E_c{}'I_c + E_sI_s$, with $E_c' = 10^3(3.32\sqrt{f_c'} + 6.90)$, (in MPa), $C_M = 1$ when the same bending moment is applied to both ends (this is the case when the load eccentricity is constant throughout the column length), while M_{pl}^s is the full plastic moment of the steel section. For the bending moment capacities M_u^c, M_u^s of the concrete and the steel parts respectively, the following expressions are suggested:

$$\begin{cases} M_u^c = \dfrac{4N_u}{0.9N_b^c}\left(1 - \dfrac{N_u}{0.9N_b^c}\right)\dfrac{C_b}{C_b + \lambda_c^2} M_0^c \\ M_u^s = \left(1 - \dfrac{N_u - N_b^c}{N_b^s}\right)\left(1 - \dfrac{N_u - N_b^c}{N_{cr}^s}\right) M_{pl}^s \end{cases} \tag{24}$$

where $M_0^c = 0.85H_c^3 f_c'/8$, N_b^c and N_b^s are the buckling capacities from equations 18 and 20 respectively, $\overline{\lambda}_c$ is found from equation 19, N_{cr}^s is the Euler load of the steel tube, M_{pl}^s is the full plastic moment of the steel section and $C_b = 0.923 - 0.0045f_c{}'$.

The ultimate compressive eccentric load N_u can be found from the above set of implicit equations, iteratively.

4. Methodology

4.1. Artificial Neural Networks

This work employs the Artificial Neural Network (ANN) technique as a means of calculation of the ultimate eccentric load of rectangular CFSTs. An ANN is a computational model inspired by biological neural networks [109], that can adapt its predictions according to observed data (a process usually called training) and make generalizations [110]. An ANN model can handle efficiently both discrete and continuous phenomena by mapping the relationships between input and output variables [111]. Complex nonlinear problems in civil engineering literature have been successfully modeled through ANNs, whereas conventional computational techniques could be hard to develop, implement or run efficiently. For example, the fire capacity of structural members was estimated by Ali et al. [112], the concrete compressive strength was predicted by Asteris and Mokos [113] and the buckling capacity of steel arch-shells was investigated by Hasanzadehshooiili et al. [114]. Among other AI-based techniques, the ANN is the prevailing model in civil engineering applications, thanks to its simplicity [115]. In its simple form an ANN model includes three distinct layers of neurons, conventionally called input, hidden and output layers. Each layer consists of a number of nodes and interconnections between each node and all the nodes in the next layer. No connection is

permitted between the nodes in the same layer however. The number of nodes in the input layer is equal to the number of input variables, while the number of nodes in the output layer coincides with the required output variables for the given problem. Any connection between nodes in the different layers represents a relationship that is described mathematically by weight and bias parameters. It is the objective of the ANN training to optimize these weights and bias so that the errors between observed and predicted outputs are minimized [116-121]. For a problem with one output response, the following nonlinear function is generalized by the ANN model [122-124]:

$$f : X \in ¡^{N} \text{ a } Y \in ¡^{1}, \tag{25}$$

where X is the input vector and Y is the predicted variable. The function f could be fully detailed, as follows [125,126]:

$$X \text{ a } f(X) = f_o\left(L_W \times \left(f_h\left(b_i + I_W \times X\right)\right) + b_o\right), \tag{26}$$

where I_W, f_h and b_i are the weight matrix, activation function and bias vector of the hidden layer; whereas L_W, f_o and b_o are the weight matrix, activation function and bias vector of the output layer, respectively.

4.2 Experimental Database

For the training and validation of the proposed ANN model as well as the comparative testing against alternative methodologies, a database of experimental tests, from the literature, has been compiled and is described here. The database contains rectangular and square CFST columns, subject to compressive loading, with and without load eccentricity. In total, 76 sources from the literature have been utilized in order to populate the database, with 1224 unique experimental specimens, outlined as:

- 880 specimens with axial concentric load
- 344 specimens with axial eccentric load.

Also, regarding the cross-section shape:

- 882 specimens with square tubes
- 342 specimens with rectangular tubes.

For the 342 strictly rectangular specimens, there is the potential to double their numbers in the database by simply alternating between their width, B and height, H dimensions. While, the physical outcome of a tested specimen having a $B \times H$ tube should not differ if the tube is described as $H \times B$, the input for these two cases to an ANN is not the same. Thus, ANN training is effectively enriched with more input data, resulting in a more experienced model. This technique has been employed in our database, resulting in additional 226 rectangular specimens (specimens with load eccentricity were omitted from this operation) and a total number equal to 882+342+226=1450 specimens.

Table **2** lists the literature sources from which the specimens in our database have been collected, along with their recorded range of ultimate compressive loads. A generic experimental setup is illustrated in Figure 4. The geometric configuration of each specimen utilizes 4

parameters:

- the steel tube section external dimensions, H and B,
- the tube wall thickness, t,
- the column effective length, L_e.
- the load eccentricity (assumed in the direction of B), e,

When load eccentricity exists, it is imposed that dimension B is parallel with eccentricity, as shown in Figure **5**. For zero eccentricity, the assignment of tube dimensions to the H and B variables is indifferent (in fact, both $H \times B$ and $B \times H$ configurations are included, as explained before). For short specimens, the effective length L_e is equal to the actual column length L. For long columns on the other hand, L_e depends on column end constraints. When it is clear from the experimental setup that free rotation is allowed at both ends, it is taken $L_e = L$. This is not always the case however. In some long specimens the experimental setup restricts rotations. The effective lengths that are reported in original sources, are used for the L_e values, in those cases.

Regarding the strength of the materials, two more parameters are recorded for each test:

- yield strength of the steel f_y,
- and the cylinder strength of the concrete f_c'.

For some specimens, the reported concrete strength was related to cube testing. For those specimens the cylinder strength in the database is reduced by a 0.85 factor[127-132]. Also, for some specimens the strength was measured using 100x200 mm cylinder molds. In these cases, the concrete strength was adjusted by a 0.92 factor, in order to become compatible to the strength measured by 150x300 mm molds that are employed in most research works.

The steel modulus of elasticity, E_s is not recorded, in an effort to keep the total number of independent variables low. This is justified by the high standardization of steel, resulting in a mostly invariant E_s value among the included specimens. In fact, for many specimens nominal E_s values are reported. Also, the concrete modulus of elasticity, E_c is not recorded because its value is connected with the strength of concrete. Both EN1992[61] and AISC360[57] provide closed-form analytical formulas for the estimation of E_c from f_c'.

Together, these 7 parameters (5 geometric, 2 material) define the input vector of each experimental test. Through this selection of parameters, crucial phenomena affecting CFST ultimate load, such as concrete confinement, section slenderness and member slenderness that are correlated to these parameters, are expected to be represented adequately in the training of the ANN model. Also, the issue of scale effect, which is observed as different concrete strength in the column compared to the measured cylinder specimens[7] is also compensated for in the model, since overall column dimensions are included as model variables. Consequently the developed ANN model expectedly should have the potential to cover these phenomena in its predictions.

In Table 3, a summary about the values input variables take in the database is presented, including minimum, maximum, mean average and standard deviation. Looking into the material strengths, it appears that both the steel yield limit f_y and the concrete compressive strength f_c' are represented through a quite wide range of input values that includes mild and high strength steels (maximum value 835 MPa) as well as normal, high strength and ultra-high strength concrete (f_c' ranging from 8.50 MPa to 168 MPa). Furthermore, the database includes a wide range of column slenderness, covering both short and long ones ($L_e/\min\{B;H\}$ ratios from 0.59

up to 49), as well as, steel section slenderness, covering both compact and slender ones ($\max\{B;H\}/t$ ratios from 10.5 up to 286).

From each experimental test one output variable is recorded. This is the ultimate compressive force, N_u, (depicted schematically in Figure 4). This is defined as the peak load throughout the loading history. In some experiments with a stable hardening branch, the peak load is realized at the end of the testing. A potential for additional loading maybe be present in these cases, however this is not recorded because the experiment is stopped typically due to excessive deformation. These tests are accepted in the database, with their end load value, considering that the potential load gain would be small at high deformations and of limited practical use. The sample of N_u values, present in the database (shown in Table 3) is considered quite extended, ranging from 105KN up to 7780 kN.

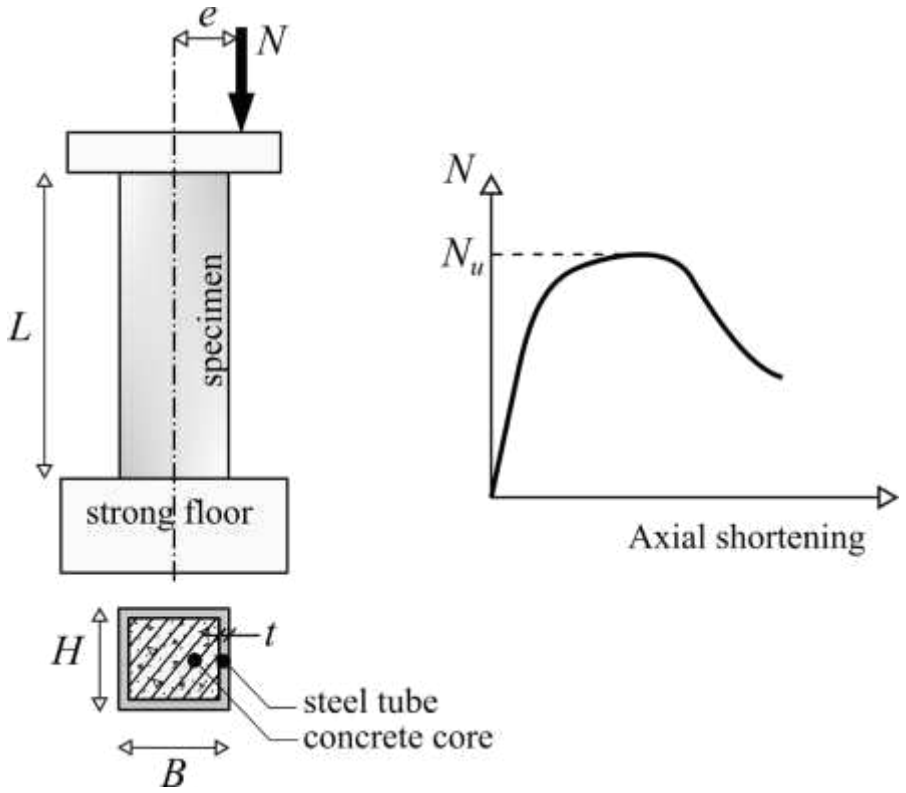

Figure 4. Rectangular Concrete-filled Steel Tube Column under compressive load, with eccentricity

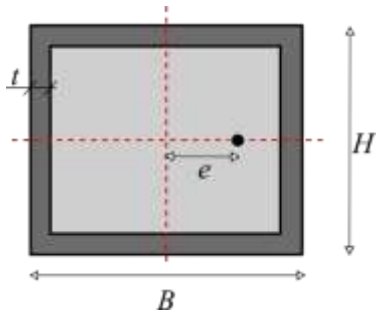

Figure 5. Definition of eccentricity e.

Table 2. Data from experiments published in literature

Nr.	Reference	Number of Samples			Axial Load	Eccentricity
		Without eccentricity	With eccentricity	Total	(kN)	(mm)
1	Zhang 1984[62]	50	-	50	660.00-2800.00	0.00
2	Lu et al. 1999[63]	6	-	6	2061.00-4872.00	0.00
3	Guo 2006[64]	6	5	11	347.00-1785.00	0.00-40.00
4	Liu & Gho 2005[65]	26	-	26	1566.00-3996.00	0.00
5	Liu et al. 2003[18]	21	-	21	1425.00-4210.00	0.00
6	Liu 2005[19]	22	-	22	1657.00-2828.00	0.00
7	Ye 2001[66]	68	-	68	1068.00-2700.00	0.00
8	Guo et al. 2006[67]	8	-	8	635.00-1785.00	0.00
9	Wei & Han 2000[68]	28	21	49	333.20-2082.50	0.00-80.00
10	Zhang & Zhou 2000[69]	36	-	36	588.00-1323.00	0.00
11	Tomii & Sakino 1979[70]	8	-	8	497.40-667.00	0.00
12	Inai & Sakino 1996[71]	46	-	46	1153.00-7780.00	0.00
13	Nakahara & Sakino 1998[72]	4	-	4	3899.00-6645.00	0.00
14	Lu & Kennedy 1992[73]	4	-	4	1906.00-4208.00	0.00
15	Yamamoto 2000[74]	16	-	16	411.00-6494.00	0.00
16	Lam & Williams 2004[75]	15	-	15	680.00-2000.00	0.00
17	Han & Yao 2004[76]	11	10	21	1415.00-2594.00	0.00-30.00
18	Matsui et al. 1995[77]	5	-	5	1143.00-1598.00	0.00
19	Furlong 1967[2]	5	-	5	488.00-1601.36	0.00
20	Grauers 1993[78]	14	-	14	1440.00-2680.00	0.00
21	Schnider 1998[79]	11	-	11	819.00-2069.00	0.00
22	Chung et al. 2001[79]	5	-	5	1144.00-1598.00	0.00
23	Han 2002[17]	4	-	4	740.00-880.00	0.00
24	Ghannam et al. 2004[81]	38	-	38	240.00-1248.00	0.00
25	Guo et al. 2005[82]	10	-	10	1558.00-2636.00	0.00

26	Luo 1986[83]	28	-	28	600.00-1740.00	0.00
27	Knowles & Park 1969[3]	6	4	10	156.35-511.55	0.00-25.40
28	Lin 1988[84]	12	-	12	558.00-1268.00	0.00
29	Khalil & Mouli 1990[85]	14	1	15	407.20-1370.00	0.00-8.00
30	Matsui & Tsuda 1996[26]	5	18	23	276.55-1597.50	0.00-125.00
31	Han & Yao 2003a[11]	19	12	31	500.00-1140.00	0.00-31.00
32	Han & Yang 2003[86]	4	-	4	490.00-825.00	0.00
33	Han & Yao 2003b[87]	6	13	19	390.00-816.00	0.00-31.00
34	Sakino et al. 2004[7]	46	-	46	1153.00-7780.00	0.00
35	Yu et al. 2008[14]	10	4	14	390.00-1220.00	0.00-30.00
36	Aslani et al. 2015[88]	12	-	12	1367.00-3882.00	0.00
37	Du et al. 2016a[89]	6	-	6	3090.00-3575.00	0.00
38	Du et al. 2016b[20]	8	-	8	1960.00-3150.00	0.00
39	Dundu 2016[15]	27	-	27	105.40-1516.26	0.00
40	Khan et al. 2017a[16]	39	-	39	286.00-6329.00	0.00
41	Khan et al. 2017b[90]	16	-	16	1636.00-7506.00	0.00
42	Mursi and Uy 2004[30]	4	4	8	1481.00-3950.00	0.00-25.00
43	Vrcelj and Uy 2002[91]	8	-	8	269.00-684.00	0.00
44	Xiong et al. 2017[92]	5	3	8	5078.00-7276.00	0.00-50.00
45	Zhu et al 2017[93]	6	-	6	2730.00-3980.00	0.00
46	Lue et al. 2007[13]	22	-	22	1281.30-2196.40	0.00
47	Liew et al. 2016[94]	5	3	8	4997.00-7276.00	0.00-50.00
48	Chen et al. 2018[10]	9	-	9	987.00-2051.00	0.00
49	Ibanez et al. 2018[21]	6	-	6	824.50-1882.50	0.00
50	Zhu and Chan 2018[95]	7	-	7	3452.00-6298.00	0.00
51	Uy 1998[6]	5	-	5	950.00-2519.00	0.00
52	Uy 2000[28]	8	12	20	619-4581.00	0.00-100.00
53	Tao et al. 2009[96]	4	-	4	1993.00-3190.00	0.00
54	Tao et al. 2008[97]	6	-	6	2140.00-4080.00	0.00

55	Cederwall et al. 1990[24]	14	12	26	610.00-2680.00	0.00-20.00
56	Chen and Jin 2010[98]	6	-	6	1980.00-2360.00	0.00
57	Han et al. 2005[99]	24	-	24	318.00-3400.00	0.00
58	Nakahara & Sakino 2000[27]	-	21	21	259.00-4100.00	45.00-300.00
59	Uy 1997[100]	-	6	6	619.00-1133.00	20.00-84.00
60	Khalil and Al-Rawdan 1996[25]	-	15	15	273.00-882.00	6.00-75.00
61	Zhang et al. 2004[31]	-	26	26	823.00-2636.00	0.90-72.00
62	Liu 2004[32]	-	12	12	660.00-1950.00	20.00-70.00
63	Guo & Zhang 2007[101]	-	2	2	655.00-983.00	30.00-40.00
64	Bridge 1976[22]	-	3	3	513.00-1956.00	38.00-64.00
65	Khalil & Zeghiche 1989[23]	-	4	4	210.00-393.00	16.00-60.00
66	Mursi & Uy 2003[29]	-	4	4	1481.00-3062.00	8.00-23.00
67	Fujimoto et al. 2004[36]	-	21	21	267.00-4045.00	45.00-300.00
68	Tao et al. 2007[102]	-	4	4	1130.00-1760.00	30.00-60.00
69	Zhang & Guo 2007[37]	-	26	26	823.00-2636.00	0.90-72.00
70	Hernandez-Figueirido et al. 2012a[103]	-	10	10	220.33-573.32	20.00-50.00
71	Hernandez-Figueirido et al. 2012b[104]	-	12	12	244.00-935.00	20.00-50.00
72	Qu et al. 2013[38]	-	9	9	750.00-3450.00	10.00-70.00
73	Lee et al. 2017[39]	-	3	3	3873.00-6491.00	20.00-40.00
74	Du et al. 2017[105]	-	12	12	2020.00-2660.00	13.00-41.50
75	Liu 2006[33]	-	20	20	617.00-1491.00	15.00-60.00
76	Li et al. 2018[41]	-	12	12	1244.10-2129.70	20.00-65.00
	Total	880	344	1224	105.40-7780.00	0.00-300.00

Table 3. The input and output parameters to be used in the development of ANN model

Nr.	Variable	Symbol	Unit	Category	Statistics			
					Min	Average	Max	STD
1	Width of Tubes Section	B	mm	Input	60.00	147.29	324.00	49.23
2	Height of Tubes Section	H	mm	Input	60.00	145.36	324.00	48.28
3	Thickness of Tubes	t	mm	Input	0.70	4.35	12.50	1.74
4	Effective Length of Column	Le	mm	Input	60.00	1109.62	4910.00	948.93
5	Steel Yield Strength	fy	MPa	Input	192.40	395.43	835.00	147.61
6	Concrete Compressive Strength	f'c	MPa	Input	8.50	51.48	168.36	27.99
7	Eccentricity	e	mm	Input	0.00	10.71	300.00	30.07
8	Axial Load	N	kN	Output	105.40	1821.84	7780.00	1394.235

The correlation between all input and output variables in the database, is further investigated through the Pearson correlation coefficient R, shown in Table 4 and graphically illustrated in Figure 6. It can be seen, that the correlation coefficient is quite low for any pair of input parameters (< 0.5), except for the high coefficient, that is observed between B and H. In general, a coefficient close to unity between input variables that implies a linear relationship between them, is problematic for the generality of the database, unless such a relationship is dictated by the actual problem. This is indeed the case between the tube dimensions B and H which practically grow in parallel, in actual CFST construction. Other than that, the stronger correlations exist between the steel and concrete strengths, f_y and f_c', with $R = 0.37$, and between the steel strength f_y and the tube thickness t, with $R = 0.42$. For the remaining pairs the coefficient is quite lower.

On the other hand, the examination of correlation between the input parameters and the output, reveals that the lower coefficients involve eccentricity e and column length L_e. The latter is decisive for the CFST ultimate load only when failure occurs by flexural buckling, instead of material yielding. Therefore, the low correlation between the N_u and L_e, indicates on one hand, that the relation between the two variables is not linear (which is true, since critical buckling load is related with the square or member length), and on the other hand, that flexural buckling is not the mode of failure for all specimens in database (which is again true, since a great number of specimens are short ones). Similarly, the low coefficient between N_u and e, is attributed to the fact that the majority of the specimens features zero eccentricity. Finally, it is worth to note that the stronger correlations between input and output variables involve the steel tube dimensions B and H, with coefficient 0.56 for both of them.

Table 4. Correlation matrix of the variables

Variables		Input Parameters							Output
		B	H	t	Le	fy	f'c	e	N
Input	B	1.00							
	H	0.71	1.00						
	t	0.14	0.11	1.00					
	Le	-0.02	-0.04	0.03	1.00				
	fy	0.05	0.04	0.42	0.06	1.00			
	f'c	-0.05	-0.05	0.22	0.07	0.37	1.00		
	e	0.25	0.21	0.08	0.12	0.03	-0.02	1.00	
Output	N	0.56	0.56	0.50	-0.18	0.52	0.40	-0.16	1.00

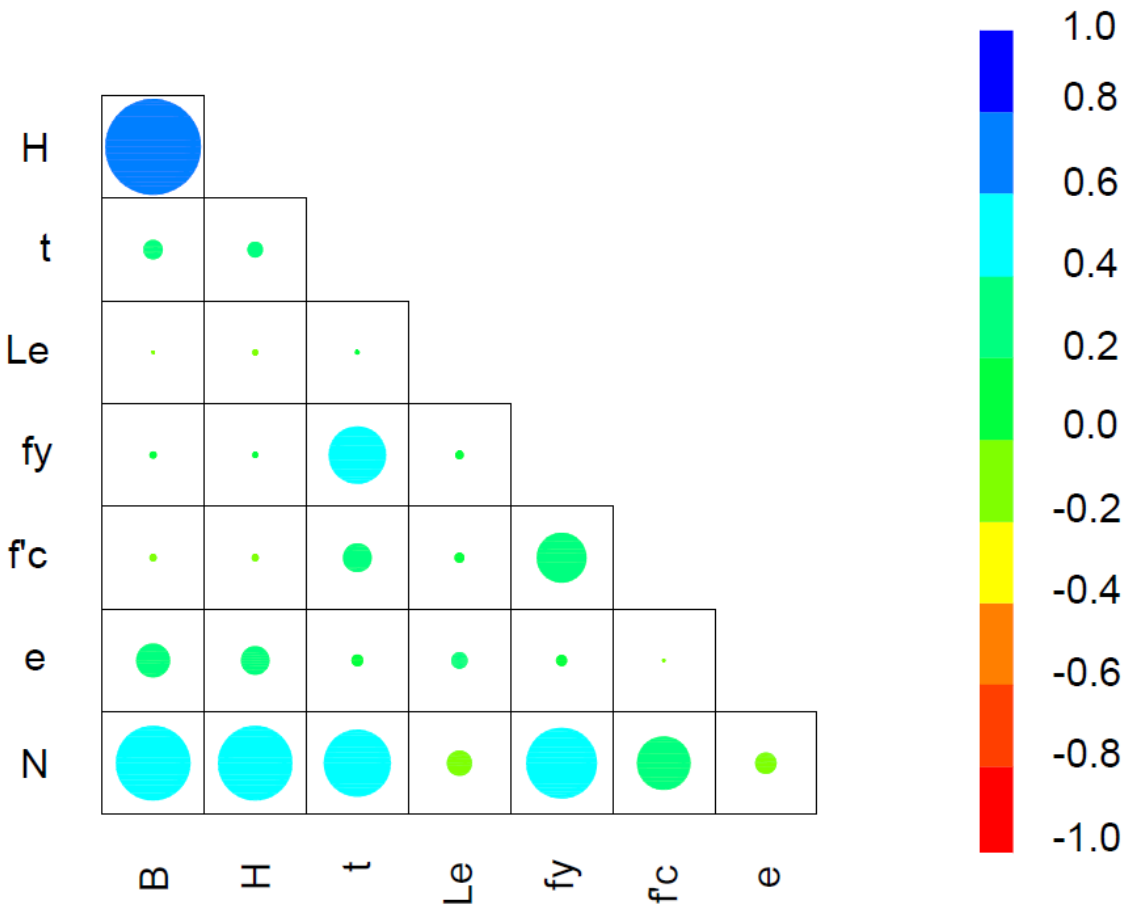

Figure 6. Correlogram of the variables (Input and Output parameters).

In Figures 3-5, scatter plots are presented between the values of input variables in the database, and the resulting output, which is the ultimate axial force N_u. Also, a histogram is presented, for each parameter (input and output) that groups its occurring values in the database, at predetermined sub-ranges. It appears from these graphs that for the steel tube dimensions, B and H, the majority of specimens utilizes lower values, mainly between 100.1 and 150mm. Higher values, are employed by gradually less specimens. In particular, a quite low number of available specimens is found in the 250.1-300mm range, which highlights the need for more experimental testing in this particular area. A similar tendency is observed for the tube thickness t, with most of the specimens utilizing values between 3.01 and 6.00mm, while only a few feature thicknesses greater than 9mm.

For the column effective length L_e, a rather strong tendency for short lengths is observed with many of the specimens constructed with lengths less than 1m. Nevertheless, a considerable number of specimens, employs longer lengths which means that the database covers member instability as a possible failure mode. To the contrary, for steel yield stress f_y, a mostly distributed scatter of its values is identified. Most specimens employ mild steels with f_y between 201MPa and 400MPa. Nevertheless, a considerable number of specimens features high strength steels, with a spike appearing in the range between 701 and 800 MPa. Similarly, a broad scatter is observed for concrete strength f_c' with most of the specimens utilizing strengths in the 21-

40MPa and secondly in the 41-60 range. For higher strengths, the number of samples in the database decreases gradually. Regarding eccentricity, the histogram shown Figure 9, reveals that the vast majority of specimens features eccentricity up to 50mm. This includes specimens with no eccentricity at all. Quite a little specimens feature larger load eccentricities, up to 300mm.

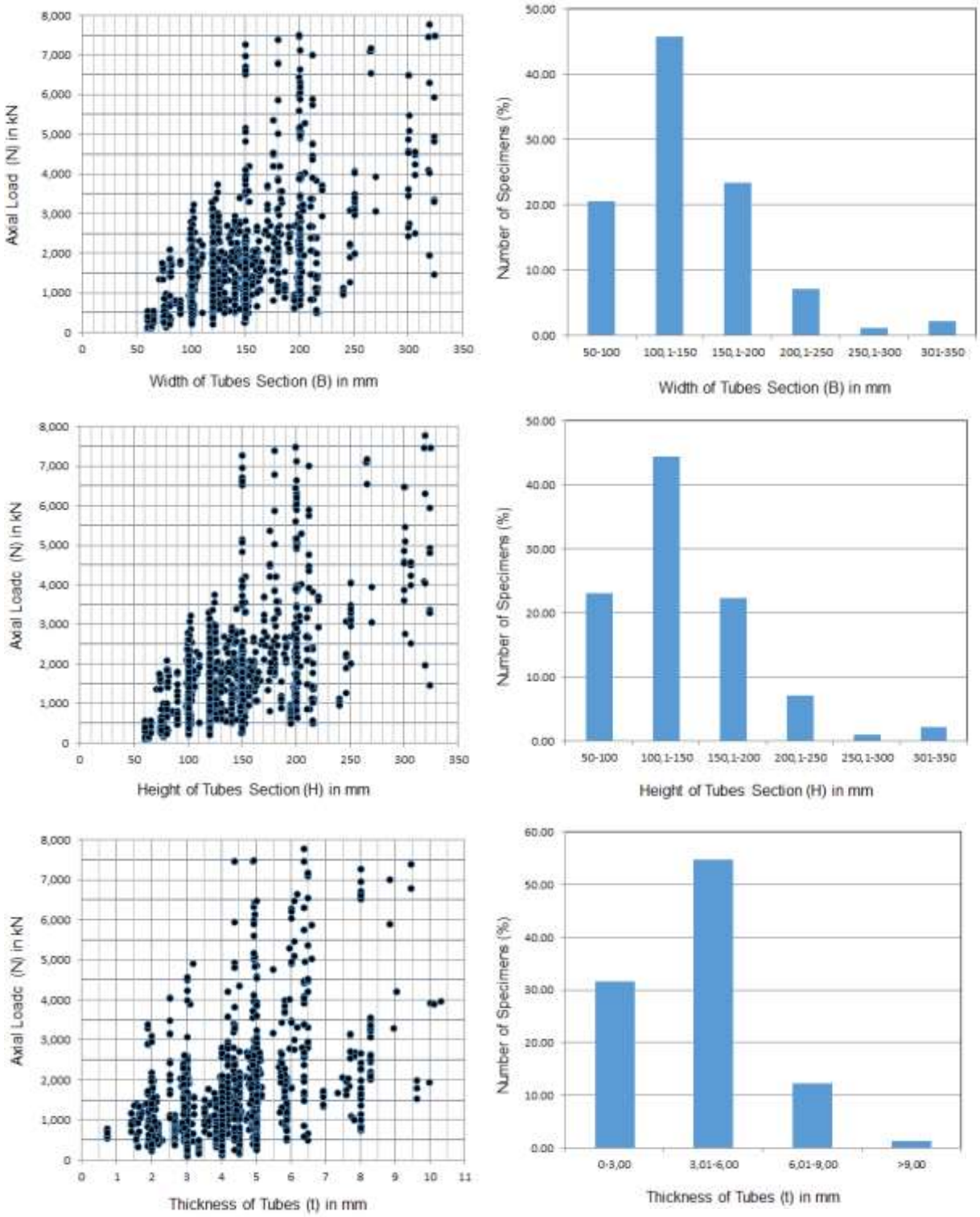

Figure 7. Histograms of the parameters: Length of Tubes Section (B); Height of Tubes Section (H); Thickness of Tubes Section (t)

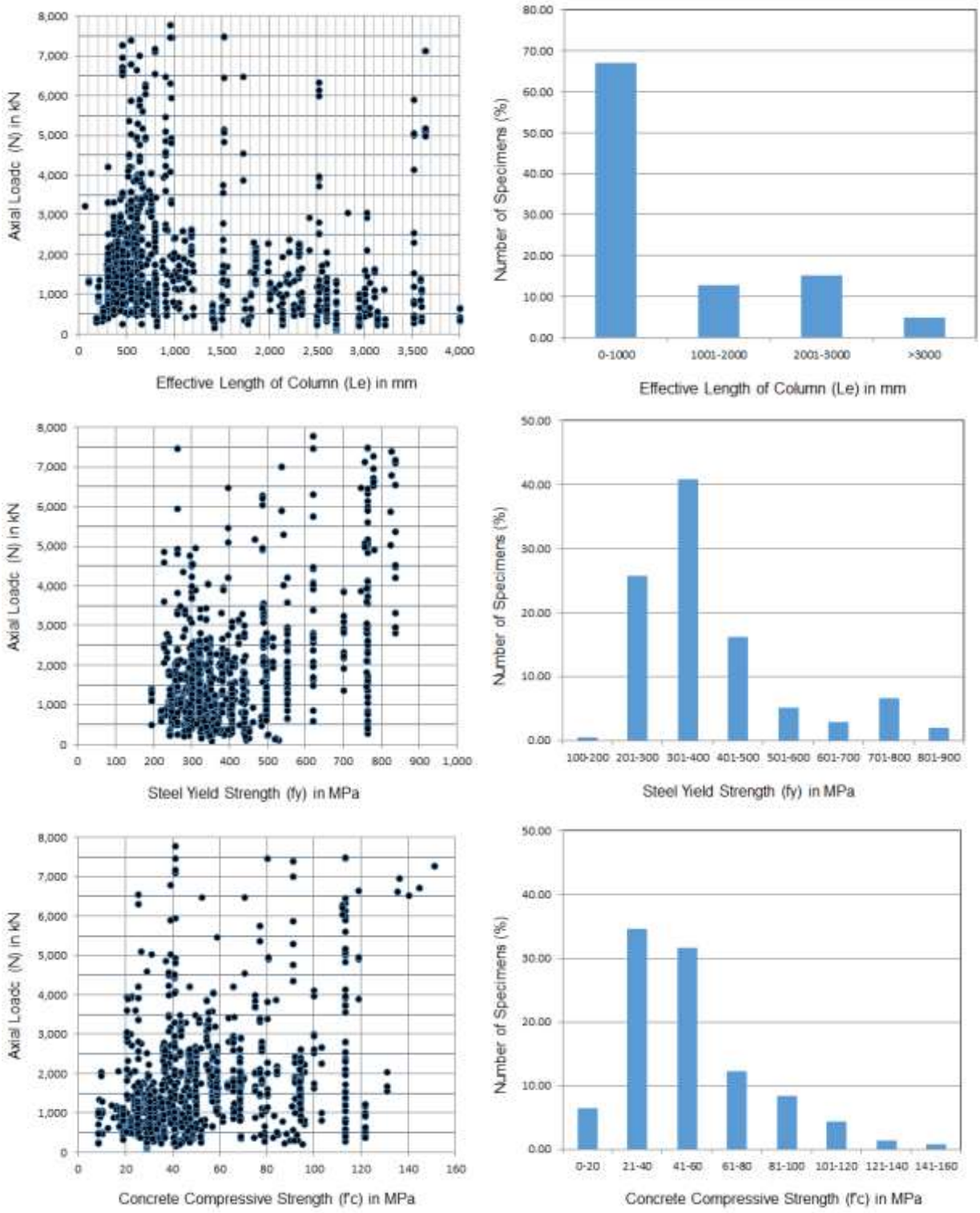

Figure 8. Histograms of the parameters: Effective Length of Steel Tube Column (L_e); Steel Yield Strength (f_y); Concrete Compressive Strength (fc');

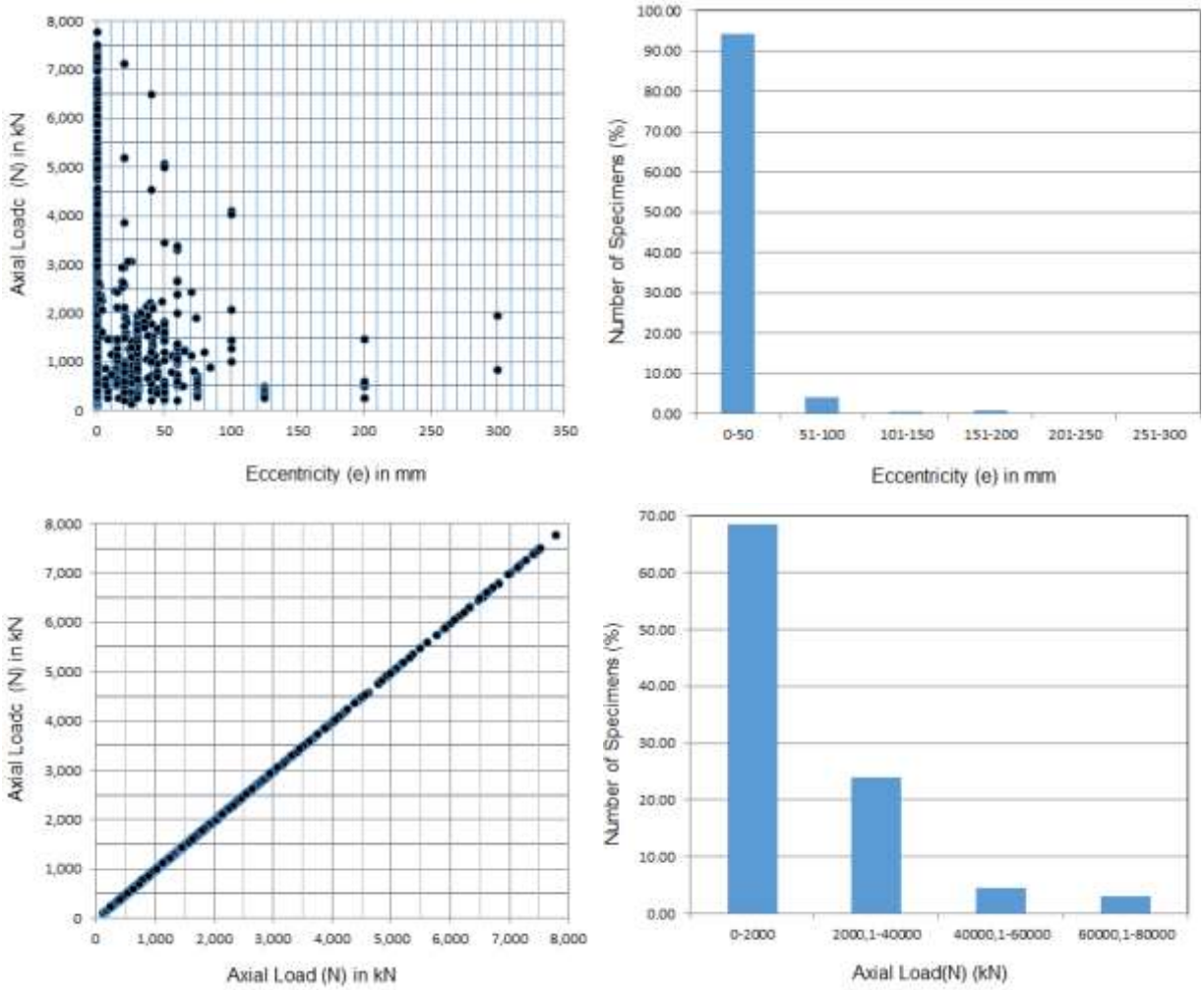

Figure 9. Histograms of the parameters: Eccentricity (e); Axial Load (N)

4.3 Sensitivity Analysis of the parameters affecting the compressive load capacity of CSFT based on the experimental database

In order to determine which of the input parameters should be included in our computational model, a sensitivity analysis (SA) was carried out. Specifically, for the specimens available in our experimental database, it is evaluated to what extend a change of any of the input parameters is manifested in the output, which is the ultimate compressive load. Excluding any input parameters that seemingly do not affect the output of the examined problem, a reduction of the overall input space can be achieved and subsequently the complexity of the model can be reduced along with the time required for its training. The SA in this work is performed using the cosine amplitude method (CAM), which is also adopted by many works in the literature [106-108]. According to the CAM, the similarity between a vector x_i that contains the values of the input variable i, for all n specimens in the database, and a vector y that contains the values of the output parameter respectively, is evaluated as:

$$R_i = \frac{\sum_{k=1}^{n} x_{ik} y_k}{\sqrt{\sum_{k=1}^{n} x_{ik}^2 \sum_{k=1}^{n} y_k^2}} \quad (27)$$

Figure 10 depicts the calculated R values between the ultimate compressive load and each of the input parameters. This analysis reveals that, the width B, the height H, the thickness t of the steel tubes and the steel yield limit f_y are ranked among the most influencing parameters on compressive load capacity values, closely followed by concrete compressive strength f_c'. The effective column length, L_e and especially the load eccentricity e demonstrate considerably lower influences. Nonzero load eccentricity however, is present only in a subset of the total sample of specimens and therefore, the observed low influence is not considered representative of the actual influence load eccentricity may have. Similarly, effective column length, L_e affects ultimate capacity only through member buckling, which is a mode of failure appearing only in long columns. Since long columns represent a subset of the entire database, the observed low influence is not considered representative of the influence column length, L_e may have on its ultimate load.

Concluding from the outcome of sensitivity analysis, it has been decided not to omit any of the examined input parameters, in the following steps of ANN model development.

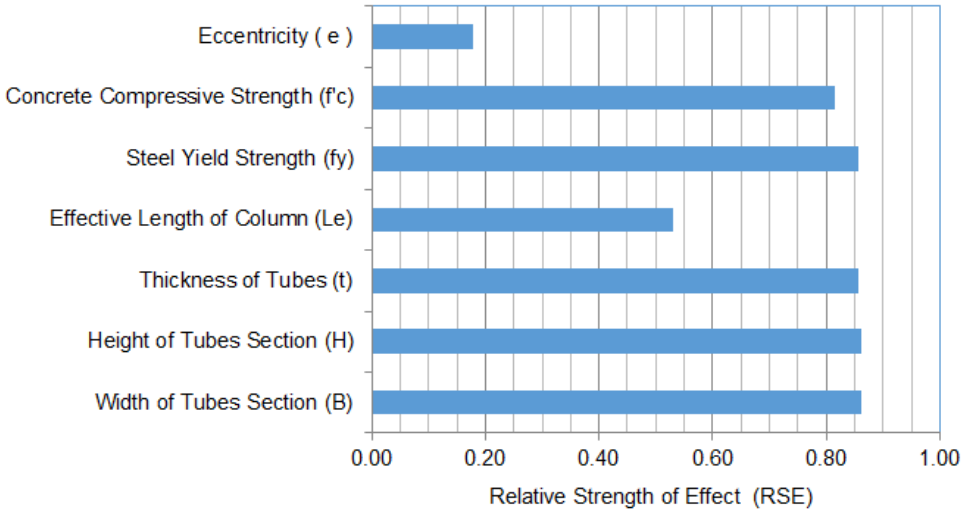

Figure 10. Sensitivity analysis of Axial Load Capacity of Rectangular Concrete-filled Steel Tube Columns

4.4 Methodology

The versatility of ANN modeling, provides a great number of parameters and options to decide upon when designing an ANN architecture for a particular problem. The selection of an optimum ANN architecture that predicts the ultimate eccentric load of CFST columns, in this paper, is not left to intuition, but it is based on a predetermined methodology that evaluates and ranks alternative architectures, according to performance metrics. Specifically, the following parameters were examined, producing numerous alternative ANN models to

evaluate:

- Normalization of data
- Number of neurons in the hidden layer
- Cost function
- Transfer function

Table **5** lists the values these parameters may take in this evaluation. The model uses one hidden layer. For the transfer function, besides the three commonly encountered Hyperbolic Tangent Sigmoid (HTS), Log-sigmoid (LS) and Linear (Li) functions, the selection includes 10 alternative functions in total, resulting to 100 (10x10) different variations for each ANN architecture. Similarly, 2 different cost functions were used and 4 different normalization techniques (including no normalization), for the input and the output parameters. The combination of all these alternatives resulted to 240.000 different ANN models. It should be noted, that the evaluation of these models was not performed over the entire sample of specimens in the database. Instead, the available data were randomly split into 3 datasets: the first dataset included 66.7% of the entire sample (967 specimens) and was reserved for the training of the alternative architectures, the second dataset included 16.7% of the entire sample (242 specimens) and was dedicated to the validation of the alternative architectures and the third dataset included the remaining 16.6% of the entire sample (241 specimens), to be used for testing and verification against other methodologies. For the splitting of the sample to the respective datasets, a programmatic procedure was used, in order to exclude potential bias. The intended reasoning behind the overall sample splitting, is to verify the generality of the evaluation of the developed model performance, against experimental data for which it was not trained.

Regarding performance metrics, five statistical indices were utilized in order to evaluate the alternative ANN architectures. These are the root mean square error (RMSE), the mean absolute percentage error (MAPE), the coefficient of determination (R^2), the variance accounted for (VAF) and the a20-index. For the RMSE and MAPE indices, lower values are better (zero means a perfect fit), while for R^2, VAF and a20-index, values closer to 1 or 100%, are wanted. The calculation of these indices is given by the following expressions:

$$\mathrm{RMSE} = \sqrt{\frac{1}{n}\sum_{i=1}^{n}(x_i - y_i)^2} \tag{28}$$

$$\mathrm{MAPE} = \frac{1}{n}\sum_{i=1}^{n}\left|\frac{x_i - y_i}{x_i}\right| \tag{29}$$

$$R^2 = 1 - \left(\frac{\sum_{i=1}^{n}(x_i - y_i)^2}{\sum_{i=1}^{n}(x_i - \bar{x})^2}\right) \tag{30}$$

$$\text{VAF} = \left(1 - \frac{Var(\boldsymbol{y} - \boldsymbol{x})}{Var(\boldsymbol{y})}\right) \times 100\% \tag{31}$$

$$\text{a20-index} = \frac{n20}{n} \tag{32}$$

where, $\boldsymbol{x}$ and $\boldsymbol{y}$ are the two vectors under comparison, in our case, $\boldsymbol{x}$ is the hidden vector of predicted by the model ultimate loads, for the n specimens in the dataset and $\boldsymbol{y}$ is the respective vector of experimental values. Also $\bar{x}$ is the mean of the $\boldsymbol{x}$ vector, var denotes the variance of a sample and $n20$ the number of specimens in $\boldsymbol{x}$ and $\boldsymbol{y}$, with $0.8 \leq y_i/x_i \leq 1.2$.

Lastly, the optimum ANN should offer numerical stability, and be free of the commonly encountered over-fitting problem. This problem results in a model that is well fitted to its calibration data, so that its performance indices are satisfactory, nevertheless, in regions of its input variables in between those provided by the calibration data, the error becomes excessive.

Table 5. Training parameters of ANN models

Parameter	Value	Matlab function
Training Algorithm	Levenberg-Marquardt Algorithm	trainlm
Normalization	Process matrices by mapping row min and max values to [0.1, 0.9] Process matrices by mapping row min and max values to [-1 1] Standardized z-scores None	mapminmax mapminmax zscore
Number of Hidden Layers	1	
Number of Neurons per Hidden Layer	1 to 30 by step 1	
Control random number generation	10 different random generation	rand(seed, generator), where generator range from 1 to 10 by step 1
Training Goal	0	
Epochs	200	
Cost Function	Mean Square Error (MSE) Sum Square Error (SSE)	mse sse
Transfer Functions	Hyperbolic Tangent Sigmoid transfer function (HTS) Log-sigmoid transfer function (LS) Linear transfer function (Li) Positive linear transfer function (PLi) Symmetric saturating linear transfer function (SSL) Soft max transfer function (SM) Competitive transfer function (Co) Triangular basis transfer function (TB) Radial basis transfer function (RB) Normalized radial basis transfer function (NRB)	tansig logsig purelin poslin satlins softmax compet tribas radbas radbasn

5. Results and Discussion

5.1 Optimum ANN model

Performing the methodology for the selection of an optimum ANN model, for the prediction of the eccentric ultimate compressive load of CFSTs, 240.000 different models were constructed and evaluated using performance indices, as described in the previous section. The top 4 ANN models among them are listed in Table 6 along with their configuration parameters and their RMSE and R^2 performance indices as well. The selected as optimum model, features a neural network structure with 21 neurons in its hidden layer (hence, called hereafter BPNN-7-21-1, with 7 being the number of input variables and 1 the number of outputs) and provides the minimum RMSE value (182.46 over the Testing Dataset) and a coefficient R2 closer to unity (0.9912 over the Testing Dataset). It also achieves the best performance indices over the Training Dataset, as well. Table **7** presents in detail all five performance indices of the selected BPNN-7-21-1 model, over three different datasets. The a20-index is over 0.90, indicating that less than 10% of the specimens were not predicted within a ±20% margin of error. Figure **11** presents graphically, the predicted vs. experimental ultimate load for different datasets of the database. A consistent behavior is observed, with the predictions closely fitted to the experimental values over the entire range of ultimate loads.

The selected BPNN-7-21-1 model employs the MinMax normalization technique, which normalizes the input and output date in the range [0.10, 0.90]. Also, it uses the Log-Sigmoid transfer function, while as cost function it uses the Mean-Square-Error (MSE). In Figure **12**, the architecture of the selected as optimum, BPNN-7-21-1 is graphically presented.

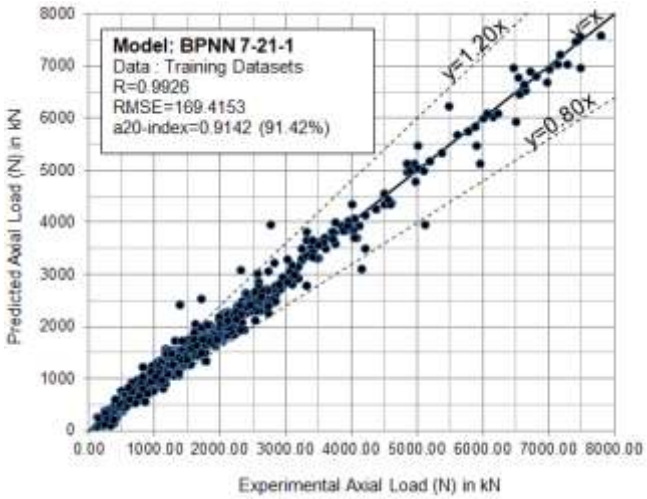

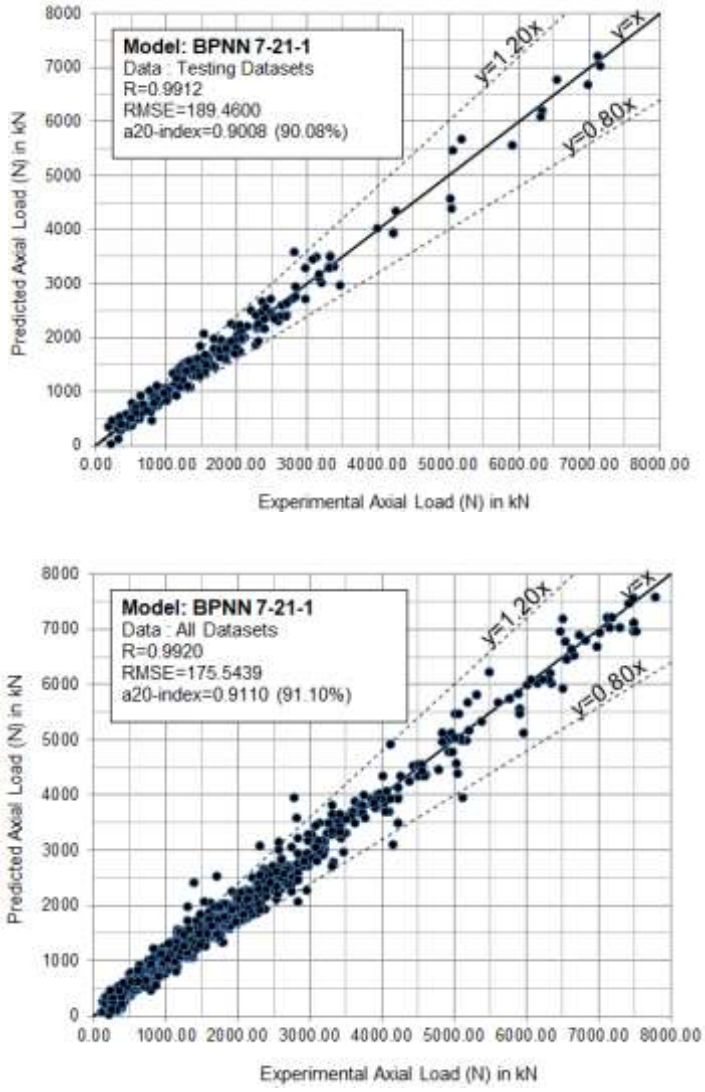

Figure 11. Experimental vs Predicted axial load for the optimum 7-21-1 BPNN

Table 6 Best ANN architectures for each one case based on RMSE performance index for Testing Datasets

Case	Architecture	Normalization	Cost Function	Transfer Function		Random Number	Epochs	Performance Indices			
								Testing Dataset		Training Dataset	
				Hidden Layer	Output Layer			R	RMSE	R	RMSE
I	7-14-1	no	MSE	PLi	PLi	7	50	0.9750	309.3980	0.9825	259.4754
II	7-26-1	Minmax [-1,1]	SSE	HTS	Li	2	12	0.9895	199.8527	0.9910	186.6267
1II	**7-21-1**	**Minmax [0.1,0.9]**	**MSE**	**LS**	**LS**	**9**	**50**	**0.9912**	**182.4600**	**0.9926**	**169.4153**
1V	7-16-1	Zscore	SSE	SM	Li	4	45	0.9906	188.3487	0.9913	183.2950

HTS : Hyperbolic Tangent Sigmoid transfer function; Li : Linear transfer function; LS : Log-Sigmoid transfer function; PLi : Positive Linear transfer function; SM : Soft Max transfer function, MSE : Mean Square Error cost function, SSE : Sum Square Error cost function.

Table 7. Summary of prediction capability of the optimum 7-21-1 BPNN

Model	**Datasets**	**Performance Indices**				
		a20-index	**R**	**RMSE**	**MAPE**	**VAF**
BPNN 7-21-1	Training	0.9142	0.9926	169.4153	0.0897	98.5199
	Testing	0.9008	0.9912	182.4600	0.1232	98.2434
	All	0.9110	0.9920	175.5439	0.0976	98.4138

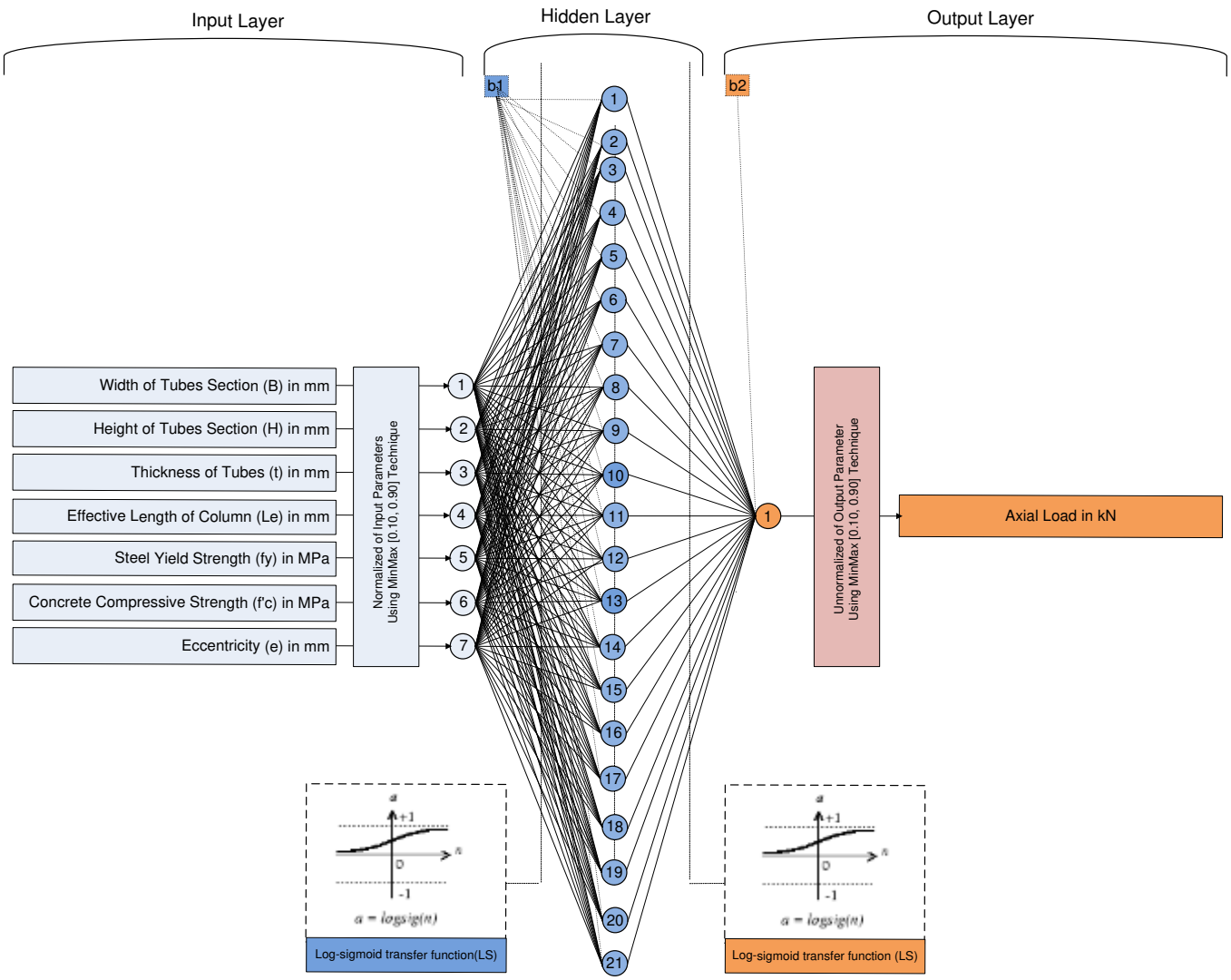

Figure 12. Architecture of the optimum BPNN-7-21-1 model

5.2 Proposed explicit equation for the estimation of ultimate load based on optimum ANN model

In a great number of existing research works investigating the training and development of artificial neural networks, the final weights and biases of the ANN model are generally not reported. As a result, it becomes difficult, if not impossible, for other researchers or engineers in design practice, to implement the proposed model in their computers, reproduce the results or further improve upon it. To remove such an obstacle, this work presents the explicit mathematical equation and the values of weights and biases, of our proposed model. Therefore, it can be readily implemented in a spreadsheet environment, by anyone interested, even without prior expertise in the field of Artificial Neural Networks.

The derived equation for the prediction of the ultimate eccentric load of rectangular CFSTs, using the width of tube section (B), the height of tube section (H), the wall thickness of the tube (t), the effective column length (L_e), the steel yield limit (f_y), the concrete cylinder compressive strength (f_c') and the eccentricity (e, aligned in parallel with width B), as input parameters, may be expressed by the following matrix:

$$\mathrm{Nu} = 7674.60(\ \mathrm{logsig}([L_W] \times [\mathrm{logsig}([I_W] \times [IP] + [b_i])] + [b_0]) - 0.1) + 105.40 \tag{33}$$

where logsig is the Log-Sigmoid transfer function; $[\mathrm{I_W}]$ is a 21×7 matrix containing the weights of the hidden layer; $[\mathrm{L_W}]$ is a 1×21 vector containing the weights of the output layer; $[\mathrm{IP}]$ is a 7×1 vector with the 7 input variables, $[\mathrm{b_i}]$ is a 21×1 vector containing the bias of the hidden layer; and $[\mathrm{b_0}]$ is a 1×1 vector containing the bias of the output layer. Equation 33 describes the developed ANN model in a purely mathematical form, making it more accessible for engineers/researchers to use in practice.

The $[\mathrm{I_W}]$ may be expressed as:

$$[I_W] = \begin{bmatrix} -3.4393 & 5.1885 & -4.8784 & 8.7376 & -0.7982 & 7.3621 & -2.0192 \\ -3.7748 & 7.6463 & -5.7352 & 8.0361 & 0.5661 & 7.2837 & -1.5192 \\ 2.4914 & 3.9003 & 7.9839 & -4.0815 & 0.3454 & -14.6014 & 4.3402 \\ -1.8008 & -0.5792 & 6.5743 & 4.2501 & -3.7633 & -3.9191 & 3.6221 \\ 3.5950 & 0.5371 & -3.1882 & 9.1113 & 6.0482 & 3.8640 & 0.8206 \\ 4.2999 & 0.6844 & -10.1837 & -0.5259 & 9.0485 & -2.3218 & 4.4721 \\ -0.2951 & 1.4285 & 2.5587 & 0.4756 & 0.1041 & 1.6523 & -13.3928 \\ -8.1957 & -5.8698 & 5.3119 & -0.7888 & 3.3607 & 3.9869 & -0.2308 \\ 9.4367 & 9.3822 & -14.2808 & -0.1092 & 24.8900 & -5.3599 & -8.6746 \\ -0.1772 & -3.9981 & -1.6608 & 9.7103 & -8.1121 & -2.7290 & -2.3057 \\ -7.6402 & 3.4071 & -1.4551 & -8.9650 & 1.3267 & 3.7606 & 3.5345 \\ 6.2607 & 4.1752 & 14.4243 & 5.4041 & 4.7285 & -18.5492 & -1.3568 \\ -5.2010 & -8.4420 & 3.1091 & 5.8518 & 0.3812 & 3.3313 & 2.8942 \\ 6.2041 & 5.7454 & -3.5953 & 14.4620 & -5.8701 & -4.1687 & -3.4684 \\ 0.4880 & -5.2763 & -3.8344 & 14.6019 & -12.1480 & -2.1766 & -3.8062 \\ 4.1697 & 0.8202 & -3.3376 & -8.7241 & 1.1267 & -6.3320 & -0.1923 \\ 1.2119 & 6.2027 & 0.5520 & -8.2085 & -5.8791 & -2.1731 & -5.0018 \\ 8.3587 & 10.5059 & -7.9431 & 0.3889 & 6.5005 & -1.7197 & -3.5586 \\ 11.7716 & -1.2101 & 12.6454 & 6.6711 & 10.4076 & 3.0460 & 0.7916 \\ -6.7804 & -7.0631 & -0.7407 & -0.2326 & -12.7946 & -12.9439 & -4.0806 \\ 8.8323 & -4.6480 & 0.1110 & -1.1300 & -2.1518 & -0.0962 & -3.5227 \end{bmatrix} \tag{34}$$

while the $[L_W]$, $[b_i]$ and $[b_0]$ may be expressed as:

$$[L_W]^T = \begin{bmatrix} -5.1947 \\ 4.6224 \\ -3.0524 \\ -1.6665 \\ -1.8181 \\ -1.0684 \\ 8.1719 \\ -1.8730 \\ 0.5569 \\ -7.2462 \\ -0.3829 \\ 0.4773 \\ -2.2391 \\ 0.9623 \\ 5.4344 \\ -9.2637 \\ -2.3014 \\ -1.3069 \\ 1.2896 \\ -0.5885 \\ 3.9043 \end{bmatrix} \quad [b_i] = \begin{bmatrix} 0.1123 \\ -0.1248 \\ -7.7443 \\ 0.3095 \\ -12.1594 \\ -0.8948 \\ -3.8988 \\ 7.0161 \\ -3.3947 \\ 8.1170 \\ 3.9961 \\ -0.5236 \\ -2.8336 \\ -1.0068 \\ 11.3124 \\ -1.8592 \\ 7.9005 \\ -2.0612 \\ -23.5287 \\ 12.0055 \\ 4.9393 \end{bmatrix} \tag{35}$$

$$[b_0] = [2.9118] \tag{36}$$

Finally, the $[IP]$ vector that contains the 7 normalized input variables (B, H, t, L_e, f_y, f_c' and e) is expressed as:

$$[IP] = \begin{bmatrix} 0.1 + \dfrac{B - 60.00}{264.00} \\ 0.1 + \dfrac{H - 60.00}{264.00} \\ 0.1 + \dfrac{t - 0.70}{11.80} \\ 0.1 + \dfrac{L_e - 60.00}{4850.00} \\ 0.1 + \dfrac{f_y - 192.40}{642.60} \\ 0.1 + \dfrac{f_c' - 8.50}{159.86} \\ 0.1 + \dfrac{e}{300} \end{bmatrix} \tag{37}$$

The included matrices above, together with equation 33, allow the implementation of the developed ANN model by researchers or software developers, facilitating its evaluation and practical utilization. It is also possible to implement the model in a spreadsheet, with a small amount of effort and time. For design purposes however, particularly in the context of code standards, a simple equation is always attractive and valuable. Nevertheless, the formulations in

existing codes, for the case of eccentrically loaded CFSTs, cannot be considered so simple and practically require a software implementation too, possibly employing iterations for the determination of internal force equilibrium. Together, with the significantly improved performance of the proposed ANN methodology, as discussed in the following section, the overall implementation requirements, using the trained ANN model, are considered rather balanced and accessible.

5.3 Comparison of ANN model with codes

In this section the performance of the developed and described previously ANN model is evaluated in comparison with existing code provisions. In Table **8**, the performance metrics are reported for the BPNN 7-21-1 model as well as for the procedures from European (EN1994[45]), American (AISC 360[57]), Japanese (AIJ[58]) and Australian/New Zealand (AS-NSZ-2327[59]) codes, omitting any safety or capacity factors, in order to obtain a more objective comparison. It should be also noted that the Japanese code procedure, that provides equation 22 for square sections only, has been adapted to cover rectangular sections too, employing rectangular stress blocks for the internal equilibrium, and using the same assumptions for the stress limits. The calculations in Table **8** have been conducted for the Testing Dataset and the presented models are sorted according to their RMSE performance.

The results in Table **8** indicate a significant overall improvement for the BPNN 7-21-1, in every performance metric. In terms of RMSE, a 43% reduction is observed from the second best, which proves the AS/NZS-2327[59] code, followed by Eurocode EN1994[45]. In terms of a20-index the improvement is also remarkable, managing to predict almost 90% of the experimental loads within a 20% error margin, compared to 77% of the specimens for the AS/NZS-2327[59] code and 75% for the Eurocode. Similar improvements can be observed for the other performance indices as well.

Among the codes, the Australian/New Zealand (AS/NZS 2327[59]) and the European (EN1994[45]) ones achieve the best overall results, with the former maintaining a slight improvement in every index. The Japanese AIJ[58]code and the American AISC 360[57] (method 2) appear quite close in terms of RMSE with a 27~28% increase compared to the Australian/New Zealand code. In terms of a20-index however the Japanese code performs slightly better whereas the American code manages the second best R index among all codes. Method 1 of the American AISC 360[57] code provide worse indices compared to Method 2, with a 4% increase in RMSE and 4% lower a20-index.

Table **9**, reports the results only for those specimens in the Testing Dataset that satisfy the field of application of the respective code (i.e. different sample for each code). For the developed BPNN 7-21-1 model the results correspond to the entire Testing Dataset. The results are again sorted according to the RMSE index. In general, a reduction of the RMSE performance index is observed for all codes. However, the proposed BPNN 7-21-1 model, performs considerably better, while still covering a broader range of input variables. In terms of RMSE, the improvement over EN1994[45], which now proves better performing, is 32%. Australian/New Zealand AS/NZS 2327 code[59] achieves a slightly increased RMSE compared to EN1994[45], however its field of application is quite broader. Other performance metrics, such as a20-index and R, are deteriorated for the codes, when their limits are considered.

Table 8. Ranking of developed soft computing BPNN 7-21-1 model against design codes, based on RMSE values for specimens in Testing Datasets

Ranking Nr.	Model	Performance Indices				
		a20-index	R	RMSE	MAPE	VAF
1	BPNN 7-21-1	0.9008	0.9912	182.4600	0.1232	98.2434
2	AS/NZS 2327	0.7686	0.9744	319.0739	0.1355	94.6993
3	EN1994	0.7469	0.9707	347.7774	0.1443	93.7929
4	AIJ	0.6488	0.9639	403.7389	0.1881	92.8971
5	AISC 360 (Method 2)	0.6281	0.9718	407.7064	0.2241	94.4157
6	AISC 360 (Method 1)	0.6017	0.9698	425.4412	0.2470	94.0270

Table 9. Ranking of developed soft computing BPNN 7-21-1 model against design codes, based on RMSE values for specimens in Testing Datasets, within code field of application.

Ranking Nr.	Model	Performance Indices				
		a20-index	R	RMSE	MAPE	VAF
1	BPNN 7-21-1	0.9008	0.9912	182.4600	0.1232	98.2434
2	EN1994	0.6500	0.9503	267.7737	0.1660	89.3850
3	AS/NZS 2327	0.7461	0.9674	274.5138	0.1391	93.5798
4	AIJ	0.5455	0.9512	302.5283	0.2102	88.3900
5	AISC 360 (Method 2)	0.5411	0.9359	388.9959	0.2572	87.0511
6	AISC 360 (Method 1)	0.5137	0.9296	407.0307	0.2843	85.9638

Figure **13**, presents the scatter plots for the experimental vs. predicted ultimate compressive load, for Testing Dataset, for the developed BPNN 7-21-1 model and also the methodologies available in design codes [45-59]. Regarding design codes, the plots include all specimens in the Validation Dataset, even if some of them do not fulfil the respective code field of application. In that case the points are drawn in gray color, whereas if they do satisfy the appropriate application limits, they are drawn in blue color. The performance of the BPNN 7-21-1 proves consistent throughout the whole range of examined load values, producing a balanced prediction average. Compared to the codes, the BPNN 7-21-1 model plot demonstrates a tighter fit, with the majority of the specimens, predicted within a 20% error margin. Comparing among the codes, a balanced prediction average is obtained using the Eurocode (EN1994[45]), the Australian/New Zealand (AS/NZS 2327[59]) and the Japanese (AIJ[58]) codes, whereas for the American code (AISC 360[57]) a systematic underestimation of the code [predicted ultimate load is observed, using either Method 1 or 2. The deviation of the points from their average seems comparable for all design codes. Also, for all the design codes, the achieved prediction error margin seems consistent throughout the entire range of examined loads, which indicates that their field of application could be extended, without affecting the prediction accuracy.

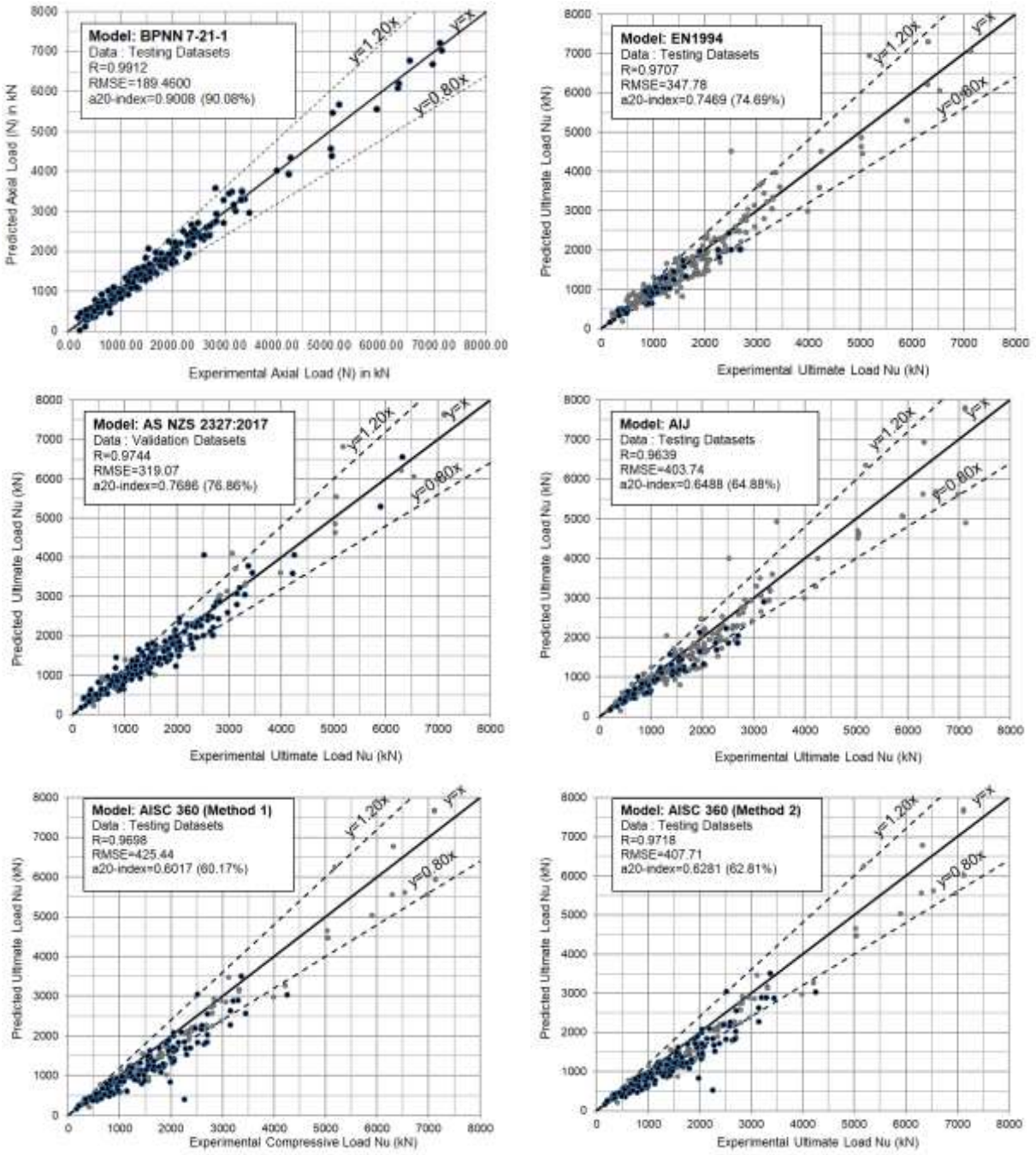

Figure 13. Comparison of developed soft computing model BPNN 7-21-1 (top left) against available procedures in design codes

In order to evaluate the behavior of the developed ANN model against parametrically with load eccentricity, a selection of specimens from the database was sought after, so that all other parameters remain constant, while the eccentricity varies. Such a requirement implies also that the selected specimens should be parts of a single testing programme, executed using the same experimental layout, batches of materials and lab equipment so that they do not differ in these aspects that remain hard to quantify their influence. In this context, a selection of 8 specimens from the work of Li et al. (2018)[41] and 20 specimens from the work of Liu (2006)[33] has been made. Table **10** presents the input parameters of the selected specimens. The 8 specimens from Li

et al. (2018)[41] employ 4 different eccentricity values (2 specimens for each eccentricity) while the specimens from Liu (2016)[33] are grouped in quadruples, each employing different cross-section dimensions, column length and a varying range of eccentricity values. It should be noted that the selected specimens do not belong to the same dataset, but some of them belong to the Training dataset, others in the Testing and others in the Validation datasets.

Table 10. Properties of selected specimens from the database for evaluation against varying eccentricity values.

Reference	**Specimens**	**Input Parameters**						
		B (mm)	**H** (mm)	**t** (mm)	**Le** (mm)	**fy** (MPa)	**fc'** (MPa)	**e** (mm)
Li et al. (2018)	EC1-EC2-EC3-EC4	150	150	4	450	434.56	93.925	20-35-50-65
Liu (2006)	S1-S2-S3-S4	120	120	4	360	495	30	15-25-30-45
	S5-S6-S7-S8	150	100	4	450	495	30	15-35-40-60
	S9-S10-S11-S12	180	90	4	540	495	30	20-30-40-50
	S13-S14-S15-S16	130	130	4	390	495	30	15-25-40-55
	L1-L2-L3-L4	150	100	4	2600	495	30	15-35-40-60

Figure **14**a depicts the ultimate load vs. eccentricity graph for the selected specimens from Li et al. (2018)[41], whereas in Figure **14**b-f the same graphs are depicted for the specimens from Liu (2006)[33]. Each graph also includes the ultimate load vs. eccentricity curves produced for the same input parameters by the developed BPNN 7-21-1 model and by the examined design codes, as well. Overall, the BPNN 7-21-1 model demonstrates a satisfactory behavior. In all cases, the produced curve is smooth and well fitted between the experimental points. The smoothness of the curve, indicates than no over-fitting occurs, a problem that can often be hiding in computational models. In the graph Figure **14**a, which is related to the Li et al (2018)[41] specimens, the BPNN 7-21-1 model, appears very consistent to predict the experimental load throughout the entire range of eccentricities. For the graphs in Figure **14**b-f, on the other hand, that are related to the Liu (2006)[33] specimens, the model underestimates the ultimate load for smaller eccentricities, while it overestimates it for larger ones. In comparison to the curves from design codes, the BPNN 7-21-1 model curve proves more successful, in all cases except, for the graph in Figure **14**f where the AS/NZS 2327 [59] and EN1994[45] models seem better fitted to the experimental values. Generally, the design codes underestimate the ultimate load whereas the BPNN 7-21-1 achieves a rather balanced averaging through the experimental points. Among the codes, the Japanese AIJ[58] and the Australian/New Zealand AS/NZS 2327[59] curves are fitted closer to the experimental codes in most cases. Considering Figure **14**f, where the BPNN 7-21-1 appears less successful, it should be noted that the specific specimens are long ones. While the database contains long specimens, the vast majority of them are short ones (see Figure **9**). Therefore, this specific outcome, can be attributed to insufficient data for training of the model in long columns. In this context, it is considered more beneficial to enrich the database with longer CFSTs than short ones, highlighting a field where future testing programmes should cover in more detail.

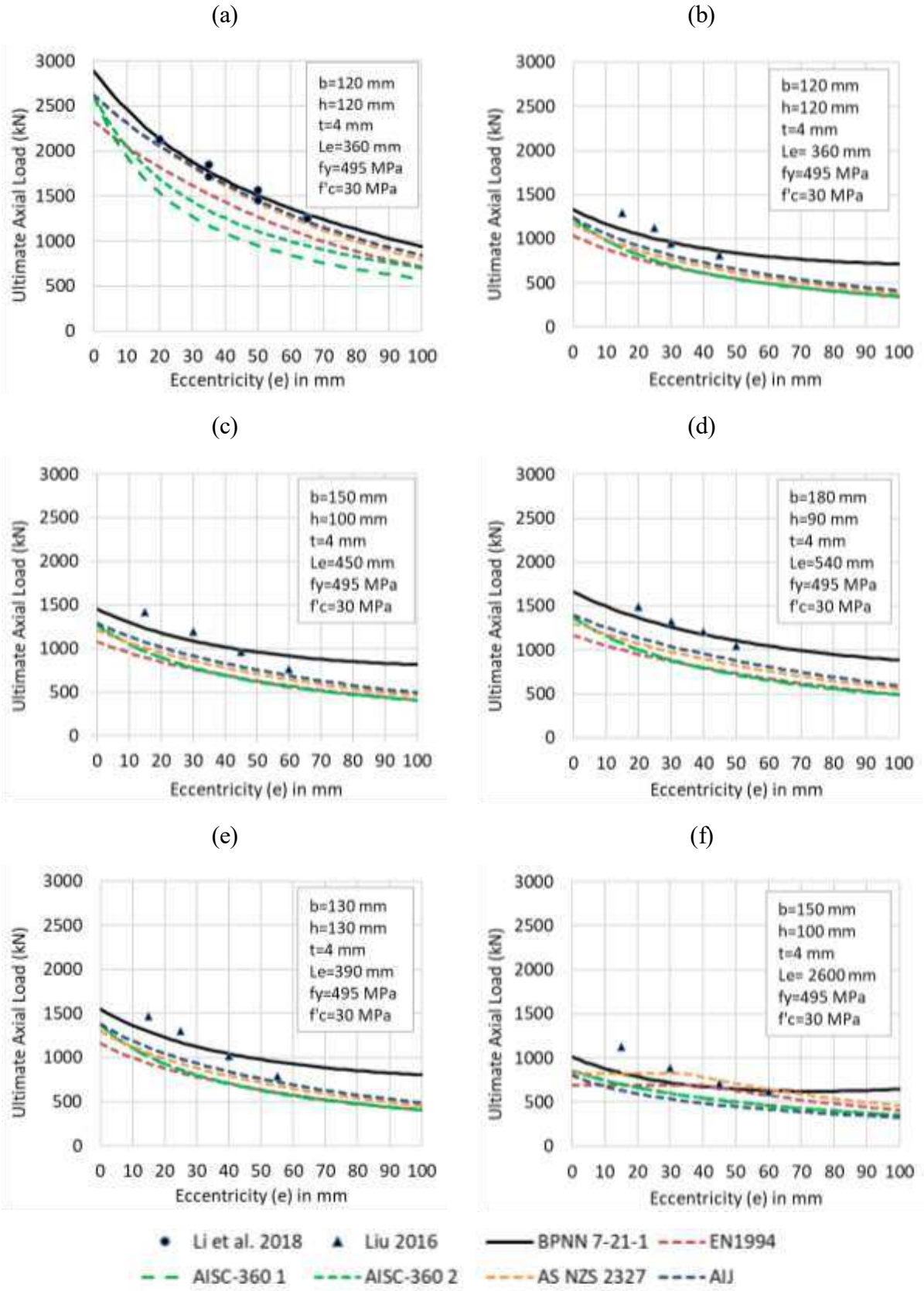

Figure 14. Comparison of the developed 7-21-1 BPNN model and code procedures against experimental specimens from the literature, for the prediction of ultimate compressive load for varying load eccentricity.

6. Conclusions

The development of a soft computing model, utilizing the artificial neural network technique, for the estimation of the ultimate eccentric load of rectangular CFST columns, was presented in this paper. To this end, an extended database of experimental tests on rectangular or square CFSTs was compiled and used for the training and validation of the model. The proposed optimum ANN architecture, was selected from numerous alternatives, with varying number of neurons, cost functions, transfer functions and normalization, on the basis of performance metrics, such as mean square error or the a20-index. The developed model takes 7 inputs, namely the tube section height, width and thickness, the column height, the steel yield limit, the concrete strength, and the eccentricity. It produces a single output, that is the ultimate compressive load. The model performance was compared to that of existing design code methodologies. The findings of the paper can be concluded to the following:

- The developed model predicts the ultimate compressive load with improved accuracy compared to existing design codes, achieving 50% reduced mean square error and significantly increased a20-index. Simultaneously, the field of application is quite extended, since the experimental sample used for its training include high strength steels, high strength concrete, slender cross sections and long columns.
- The developed ANN model features only 1 hidden layer with 21 neurons, yet it manages to the model the behavior of CFSTs in a wide field of application, that covers standard and high strength materials, compact and slender tube sections and short or long columns, highlighting the versatility and effectiveness of the approach.
- By examination of the developed model against selected individual experimental specimens, its numerical stability was verified and found free of any overfitting problems, The model produced better fitting to the experimental data, particularly for short columns.
- Performing a sensitivity analysis, over the collected experimental tests, it was found that the most influencing parameters for the ultimate compressive load are the steel tube dimensions, its thickness and the material strengths as well. All those parameters, produced rather close values of correlation with the resulting ultimate load.

The proposed ANN model produces a single output, which is the ultimate compressive load, accounting for load eccentricity. In this context, valuable output could also be the axial load vs moment interaction diagram. Furthermore, for the needs of nonlinear analysis, a more detailed output is required, which can include the entire load vs deformation curve. These aspects of the CFST response, together with further enrichment of the experimental database are reserved for future research.

While the entire process of ANN model development and verification is indeed complicated and requires a level of expertise on numerical computing, its application and use for the design of actual structures is not. The model can be easily implemented in a spreadsheet or any other programming environment, using the provided weights and biases. Compared to the procedures provided by design codes, that often require an iterative process in order to determine the

equilibrium of internal forces inside the cross section, under conditions of combined axial force and bending moment, the programming of the ANN model instead, could be more straightforward while the computing time it requires is constant and potentially less.

Conflicts of Interest: The authors declare that there is no conflict of interest regarding the publication of this paper.

Data Availability: The raw/processed data required to reproduce these findings will be made available on request.

Funding Statement: This research received no external funding.

Supplementary material: The Excel-based Graphical User Interface for prediction of axial compressive load of CFST columns, based on the optimal machine learning model is appended to this paper.

References

1. Kloppel VK, Goder W. (1957). An investigation of the load carrying capacity of concrete-filled steel tubes and development of design formula, Der Stahlbau, Vol. 26(1), pp. 1-10.
2. Furlong RW. (1967). Strength of steel-encased concrete beam columns. Journal of the Structural Division, Vol. 93(5), pp. 113-124.
3. Knowles RB, Park R. (1969). Strength of Concrete Filled Steel Tubular Columns. Journal of the Structural Division, Vol. 95(12), pp. 2565-88.
4. Gardner NJ, Jacobson ER. (1967). Structural behavior of concrete filled steel tubes, ACI Journal, Vol. 64(7), pp. 404-413.
5. Tomii, M. (1977). Experimental studies on concrete filled steel tubular stub columns under concentric loading, In: Proceedings of International Colloquium on Stability of Structures Under Static and Dynamic Loads, SSRC/ASCE/Washington, DC, pp.718-41.
6. Uy, B. (1998). Local and post-local buckling of concrete filled steel welded box columns. Journal of Constructional Steel Research, Vol. 47(1-2), pp.47-72.
7. Sakino K, Nakahara H, Morino S, Nishiyama I. (2004). Behavior of Centrally Loaded Concrete-Filled Steel-Tube Short Columns, Journal of Structural Engineering, Vol.130(2), pp.180-88.
8. Chitawadagi, M. V., Narasimhan, M. C., & Kulkarni, S. M. (2010). Axial capacity of rectangular concrete-filled steel tube columns–DOE approach. Construction and Building Materials, 24(4), 585-595.
9. Evirgen, B., Tuncan, A., & Taskin, K. (2014). Structural behavior of concrete filled steel tubular sections (CFT/CFSt) under axial compression. Thin-Walled Structures, 80, 46-56.
10. Chen S, Zhang R, Jia LJ, Wang JY and Gu P. (2018). Structural behavior of UHPC filled steel tube columns under axial loading. Thin-Walled Structures, Vol.130,

pp.550-563.
11. Han, L. H., & Yao, G. H. (2003). Influence of concrete compaction on the strength of concrete-filled steel RHS columns. Journal of Constructional Steel Research, 59(6), 751-767.
12. Mursi M, Uy B. (2004). Strength of slender concrete filled high strength steel box columns, Journal of Constructional Steel Research, Vol. 60, pp. 1825-48.
13. Lue, D. M., Liu, J. L., & Yen, T. (2007). Experimental study on rectangular CFT columns with high-strength concrete. Journal of Constructional Steel Research, 63(1), 37-44.
14. Yu, Q., Tao, Z. and Wu, Y.X., (2008). Experimental behaviour of high performance concrete-filled steel tubular columns. Thin-Walled Structures, Vol. 46(4), pp.362-370.
15. Dundu M. (2016). Column buckling tests of hot-rolled concrete filled square hollow sections of mild to high strength steel, Engineering Structures, Vol. 127, pp. 73-85.
16. Khan M, Uy B, Tao Z, Mashiri F. (2017). Concentrically loaded slender square hollow and composite columns incorporating high strength properties, Engineering Structures, Vol. 131, pp. 69-89.
17. Han LH. (2002). Tests on stub columns of concrete-filled RHS sections, Journal of Constructional Steel Research, Vol. 58(3), pp. 353-372.
18. Liu D, Gho WM, Yuan J. (2003). Ultimate capacity of high-strength rectangular concrete-filled steel hollow section stub columns, Journal of Constructional Steel Research, Vol. 59(12), pp. 1499-1515.
19. Liu D. (2005). Tests on high-strength rectangular concrete-filled steel hollow section stub columns, Journal of Constructional Steel Research, Vol. 61(7), pp. 902-11.
20. Du Y, Chen Z, Yu Y (2016). Behavior of rectangular concrete-filled high-strength steel tubular columns with different aspect ratio, Thin-Walled Structures, Vol. 109, pp. 304-18.
21. Ibañez C, Hernández-Figueirido D, Piquer A. (2018). Shape effect on axially loaded high strength CFST stub columns, Journal of Constructional Steel Research, Vol. 147, pp.247-56.
22. Bridge RQ, (1976). Concrete Filled Steel Tubular Columns, University of Sydney, Department of Civil Engineering, Research Report No. R283.
23. Khalil SH and Zeghiche Z. (1989). Experimental Behaviour of Concrete-Filled Rolled Rectangular Hollow-Section Columns, The Structural Engineer, v. 67(19), pp. 345–353.
24. Cederwall, K., Engstrom, B. and Grauers, M. (1990). High-Strength Concrete Used in Composite Columns, SP, vol. 121, pp. 195–214.
25. Khalil SH and Al-Rawdan A. (1996). Behaviour of Asymmetrically Loaded Concrete-Filled Tubular Columns, In: Proceedings of the Seventh International Symposium on Tubular Structures, Farkas J. and Jarmai, K. (eds.), University of Miskolc, Hungary, pp. 363–370
26. Matsui, C. and Tsuda, K. (1996). Strength And Behavior Of Slender Concrete Filled Steel Tubular Columns, Proceedings of The Second International Symposium on Civil Infrastructure Systems, P.T.Y. Chang, L. W. Lu, and L. Wei, eds., Hong Kong, China., 1996.

27. Nakahara H., Sakino K.. (2000) Practical Analysis for High Strength CFT Columns under Eccentric Compression, In: Proceedings of the Sixth ASCCS International Conference on Steel-Concrete Composite Structures, Xiao, Y. and Mahin, S. A. (eds.), Los Angeles, California, March 22-24, 2000.
28. Uy, B. (2000). Strength of concrete filled steel box columns incorporating local buckling. Journal of Structural Engineering, 126(3), 341-352.
29. Mursi M, Uy B. (2003). Strength of concrete filled steel box columns incorporating interaction buckling, Journal of Structural Engineering, Vol. 129, pp. 626-39.
30. Mursi M, Uy B. (2004). Strength of slender concrete filled high strength steel box columns, Journal of Constructional Steel Research, Vol. 60, pp. 1825-48.
31. Zhang S, Guo L, Wang Y, and Tian H. (2004). Experimental research and theoretical analysis on high-strength concrete-filled SHS steel tubes subjected to eccentric load, Journal of Building Structures, Vol. 25(1), pp. 17–24.
32. Liu D. (2004). Behaviour of high strength rectangular concrete-filled steel hollow section columns under eccentric loading, Thin-walled structures, Vol. 42(12), pp. 1631-1644.
33. Liu D. (2006). Behaviour of eccentrically loaded high-strength rectangular concrete-filled steel tubular columns. Journal of Constructional Steel Research, Vol. 62(8), pp. 839-846.
34. Varma AH, Ricles JM, Sause R, Lu L-W. (2002). Experimental behaviour of high strength square concrete-filled steel tube beam-columns, Journal of Structural Engineering, Vol.128(3), pp.309-18.
35. Varma AH, Ricles JM, Sause R, Lu LW. (2004). Seismic behavior and design of high-strength square concrete-filled steel tube beam columns. Journal of Structural Engineering, Vol. 130(2), pp. 169-179.
36. Fujimoto T, Mukai A, Nishiyama I, Sakino K. (2004). Behavior of eccentrically loaded concrete-filled steel tubular columns. Journal of Structural Engineering, Vol. 130(2), pp. 203-212.
37. Zhang S, Guo L. (2007). Behaviour of high strength concrete-filled slender RHS steel tubes. Advances in Structural Engineering, Vol. 10(4), pp. 337-351.
38. Qu X, Chen Z, Sun G. (2013). Experimental study of rectangular CFST columns subjected to eccentric loading, Thin-Walled Structures, Vol. 64, pp. 83-93.
39. Lee HJ, Choi IR, Park HG. (2017). Eccentric compression strength of rectangular concrete-filled tubular columns using high-strength steel thin plates, Journal of Structural Engineering, Vol. 143(5), p. 04016228.
40. Du Y, Chen Z, Liew JR, Xiong MX. (2017). Rectangular concrete-filled steel tubular beam-columns using high-strength steel: experiments and design. Journal of constructional steel research, Vol. 131, pp. 1-18.
41. Li G, Chen B, Yang Z, Feng Y. (2018). Experimental and numerical behaviour of eccentrically loaded high strength concrete filled high strength square steel tube stub columns, Thin-Walled Structures, Vol. 127, pp. 483-499.
42. Patel, V. I., Liang, Q. Q., & Hadi, M. N. (2012a). High strength thin-walled rectangular concrete-filled steel tubular slender beam-columns, Part I: Modeling. Journal of Constructional Steel Research, 70, 377-384.

43. Patel, V. I., Liang, Q. Q., & Hadi, M. N. (2012b). High strength thin-walled rectangular concrete-filled steel tubular slender beam-columns, Part II: Behavior. Journal of Constructional Steel Research, 70, 368-376.
44. Patel, V. I. (2020). Analysis of uniaxially loaded short round-ended concrete-filled steel tubular beam-columns. Engineering Structures, 205, 110098.
45. Güneyisi, E. M., Gültekin, A., & Mermerdaş, K. (2016). Ultimate capacity prediction of axially loaded CFST short columns. International Journal of Steel Structures, 16(1), 99-114.
46. Du, Y.; Chen, Z.; Zhang, C.; Cao, X. Research on axial bearing capacity of rectangular concrete-filled steel tubular columns based on artificial neural networks. Frontiers of Computer Science 2017, 11, 863–873.
47. Jayalekshmi, S., Jegadesh, J. S., & Goel, A. (2018). Empirical approach for determining axial strength of circular concrete filled steel tubular columns. Journal of The Institution of Engineers (India): Series A, 99(2), 257-268.
48. Tran, V. L., Thai, D. K., & Kim, S. E. (2019). Application of ANN in predicting ACC of SCFST column. Composite Structures, 228, 111332.
49. Ren, Q., Li, M., Zhang, M., Shen, Y., & Si, W. (2019). Prediction of ultimate axial capacity of square concrete-filled steel tubular short columns using a hybrid intelligent algorithm. Applied Sciences, 9(14), 2802.
50. Le, T. T., & Phan, H. C. (2020). Prediction of Ultimate Load of Rectangular CFST Columns Using Interpretable Machine Learning Method. Advances in Civil Engineering, 2020.
51. Zarringol, M., Thai, H. T., Thai, S., & Patel, V. (2020, December). Application of ANN to the design of CFST columns. In Structures (Vol. 28, pp. 2203-2220). Elsevier.
52. Javed, M. F., Farooq, F., Memon, S. A., Akbar, A., Khan, M. A., Aslam, F., ... & Rehman, S. K. U. (2020). New prediction model for the ultimate axial capacity of concrete-filled steel tubes: An evolutionary approach. Crystals, 10(9), 741.
53. Naser, M. Z., Thai, S., & Thai, H. T. (2021). Evaluating structural response of concrete-filled steel tubular columns through machine learning. Journal of Building Engineering, 34, 101888.
54. Asteris PG, Lemonis ME, Nguyen TA, Le HV and Pham BT. (2021). Soft computing-based estimation of ultimate axial load of rectangular concrete-filled steel tubes, Steel and Composite Structures, Volume 39, Number 4, pp 471-491, DOI: http://dx.doi.org/10.12989/scs.2021.39.4.471
55. Le TT, Asteris PG and Lemonis ME. (2021). Prediction of Axial Load Capacity of Rectangular Concrete-filled Steel Tube Columns using Machine Learning Techniques, Engineering with Computers, in press
56. Eurocode 4, CEN, EN1994-1, (2004), Design of composite steel and concrete structures - Part 1-1: General Rules and Rules for Buildings, Brussels, Belgium.
57. AISC (2016), Specification for structural steel buildings ANSI/AISC 360-16; American Institute of Steel Construction: Chicago, USA
58. AIJ (1997), A.I. of Recommendations for design and construction of concrete filled steel tubular structures; Architectural Institute of Japan, Japan
59. AS/NZS 2327 (2017), Composite structures-Composite steel concrete construction in

buildings; Australian/New Zealand Standard.
60. Eurocode 3, CEN, EN1993-1, (2005), Design of steel structures - Part 1-1: General Rules and Rules for Buildings, Brussels, Belgium.
61. Eurocode 2, CEN, EN1992-1, (2004), Design of concrete structures - Part 1-1: General Rules and Rules for Buildings, Brussels, Belgium.
62. Zhang Z. (1984). Experimental research on short filled concrete square steel tube columns under axial compressive load, Masters thesis, Harbin University of Technology, Harbin, China.
63. Lu X, Yu Y, Chen Y. (1999). Studies on the behavior of concrete-filled rectangular tubular short column: 1 Experiment, Building Structures, China, vol. 29, no. 10, pp. 41–43.
64. Guo L. (2006). Theoretical and experimental reearch on the behavior of concrete-filled rectangular hollow section steel tubes, PhD thesis, Harbin Institute of Technology, Harbin, China.
65. Liu D, and Gho WM. (2005). Axial load behaviour of high-strength rectangular concrete-filled steel tubular stub columns. Thin-Walled Structures, 43(8), 1131-1142.
66. Ye Z. (2001). Conpressive behavior of high-strength concrete-filled square and rectangular steel tubes, Masters thesis, Harbin Institute of Technology, Harbin, China.
67. Guo LH, Zhang SM, Kim WJ. (2006). Elastic and elastic-plastic buckling behavior of SHS steel tube filled with concrete, Harbin Gongye Daxue Xuebao/Journal of Harbin Institute of Technology, Vol. 38, no. 8, pp. 1350–1354.
68. Wei Z, and Han L. (2000). Research on the bearing capacity of early-strength concrete filled square steel tube, Proceedings 6th ASCCS Conference; Composite and Hybrid Structures, Vol. 1, Los Angeles, pp. 395–402, 2000.
69. Zhang S, and Zhou M. (2000). Stress-strain behavior of concrete-filled square steel tubes, Proceedings 6th ASCCS Conference; Composite and Hybrid Structures, Vol. 1, Los Angeles, pp. 403–410.
70. Tomii M, and Sakino K. (1979). Experimental studies on the ultimate moment of concrete filled square steel tubular beam-columns., Transactions of the Architectural Institute of Japan, no. 275, pp. 55–65.
71. Inai E, and Sakino K. (1996). Simulation of Flexural Behavior of Square Concrete Filled Steel Tubular Columns, Proceedings of the Third Joint Technical Coordinating Committee Meeting, U.S.-Japan Cooperative Research Program, Phase 5: Composite and Hybrid Structures, Hong Kong, National Science Foundation, Arlington, Virginia.
72. Nakahara H, and Sakino K. (1998). Axial Compressive and Uniform Bending Tests of High Strength Concrete Filled Square Steel Tubular Columns, Proceedings of the Fifth Pacific Structural Steel Conference, Seoul, Korea, pp. 943–948.
73. Lu YQ, and Kennedy DJL. (1994). The flexural behaviour of concrete-filled hollow structural sections, Can. J. Civ. Eng., Vol. 21, no. 1, pp. 111–130.
74. Yamamoto T, Kawaguchi J, Morino S. (2000). Experimental Study of Scale Effects on the Compressive Behavior of Short Concrete-Filled Steel Tube Columns, Proc. of Composite Construction in Steel and Concrete IV, 879-890, May 28-June 2, 2000, Banff, Alberta, Canada.
75. Lam D, Williams CA. (2004). Experimental study on concrete filled square hollow

sections, Steel and Composite Structures, Vol. 4(2), pp.95-112
76. Han LH, and Yao GH. (2004). Experimental behaviour of thin-walled hollow structural steel (HSS) columns filled with self-consolidating concrete (SCC). Thin-Walled Structures, Vol. 42(9), pp. 1357-1377.
77. Matsui, C., Tsuda, K. and Ishibashi, Y. (1995). Slender concrete filled steel tubular columns under combined compression and bending, Structural Steel, PSSC95, 4th Pacific Structural Steel Conference, Vol. 3, Steel- Concrete Composite Structures, Singapore, pp. 29–36, 1995.
78. Grauers, M. (1993). Composite columns of hollow steel sections filled with high strength concrete, Göteborg, Chalmers Univ. of Technology, Diss. : 1993, 1993.
79. Schneider, S.P. (1998). Axially Loaded Concrete-Filled Steel Tubes," Journal of Structural Engineering, vol. 124, no. 10, pp. 1125–1138.
80. Chung, J., Matsui, C. and Tsuda, K. (2001). Simplified design formula of slender concrete filled steel tubular beam-columns, Structural Engineering and Mechanics, vol. 12, no. 1, pp. 71–84.
81. Ghannam, S., Jawad, Y.A. and Hunaiti, Y. (2004). Failure of lightweight aggregate concrete-filled steel tubular columns, Steel and Composite Structures, vol. 4, no. 1, pp. 1–8.
82. Guo, L., Zhang, S., Wang, Y. and Liu, J. (2005). Analytical and experimental research on axially loaded slender HSC filled RHS steel tubular columns, Industrial Construction, China, vol. 35, no. 3, pp. 75–79.
83. Luo, L. (1986). Experimental research on long filled concrete square steel tube columns under axial compressive load, Masters thesis, Zheng Zhou University of Technology, 1986.
84. Lin, C.Y. (1988). Axial Capacity of Concrete Infilled Cold-Formed Steel Columns, Ninth International Specialty Conference on Cold-Formed Steel Structures, St. Louis, Missouri, U.S.A., pp. 443–457, 1988.
85. Khalil SH. and Mouli M. (1990). Further Tests on Concrete-Filled Rectangular Hollow-Section Columns, The Structural Engineer, vol. 68, no. 20, pp. 405–413.
86. Han, L.-H. and Yang, Y.-F. (2003). Analysis of thin-walled steel RHS columns filled with concrete under long-term sustained loads, Thin-Walled Structures, vol. 41, no. 9, pp. 849–870.
87. Han, L. H., & Yao, G. H. (2003). Behaviour of concrete-filled hollow structural steel (HSS) columns with pre-load on the steel tubes. Journal of Constructional Steel Research, 59(12), 1455-1475.
88. Aslani F, Uy B, Tao Z, Mashiri F. (2015). Behaviour and design of composite columns incorporating compact high-strength steel plates, Journal of Constructional Steel Research, Vol. 107, pp. 94-110.
89. Du Y, Chen Z, and Xiong MX, (2016). Experimental behavior and design method of rectangular concrete-filled tubular columns using Q460 high-strength steel. Construction and Building Materials, Vol. 125, pp.856-872.
90. Khan M, Uy B, Tao Z, Mashiri F. (2017). Behaviour and design of short high-strength steel welded box and concrete-filled tube (CFT) sections, Engineering Structures, Vol. 147, pp. 458-472.

91. Vrcelj, Z. and Uy, B. (2002). Behaviour and Design of Steel Square Hollow Sections Filled With High Strength Concrete, Australian Journal of Structural Engineering, vol. 3, no. 3, pp. 153–170.
92. Xiong MX, Xiong DX, Liew JR. (2017). Axial performance of short concrete filled steel tubes with high-and ultra-high-strength materials, Engineering Structures, Vol. 136, pp. 494-510.
93. Zhu A, Zhang X, Zhu H, Zhu J, Lu Y. (2017). Experimental study of concrete filled cold-formed steel tubular stub columns, Journal of Constructional Steel Research, Vol. 134, pp. 17-27.
94. Liew JR, Xiong M, Xiong D. (2016). Design of concrete filled tubular beam-columns with high strength steel and concrete, Structures, Vol. 8, pp. 213-226.
95. Zhu, Jiong-Yi, and Tak-Ming Chan. (2018). Experimental investigation on octagonal concrete filled steel stub columns under uniaxial compression, Journal of constructional steel research, Vol. 147, pp. 457-467.
96. Tao Z, Uy B, Han LH, Wang ZB. (2009). Analysis and design of concrete-filled stiffened thin-walled steel tubular columns under axial compression, Thin-Walled Structures, Vol. 47, pp. 1544-1556
97. Tao, Z., Han, L. H., & Wang, D. Y. (2008). Strength and ductility of stiffened thin-walled hollow steel structural stub columns filled with concrete. Thin-walled structures, 46(10), 1113-1128.
98. Chen, J. and Jin, W. (2010). Experimental investigation of thin-walled complex section concrete-filled steel stub columns, Thin-Walled Structures, vol. 48, no. 9, pp. 718–724.
99. Han LH, Yao GH. Zhao XL. (2005). Tests and calculations for hollow structural steel (HSS) stub columns filled with self-consolidating concrete (SCC). Journal of Constructional Steel Research, Vol. 61, pp.1241-1269
100. Uy B. (1997). Ductility and strength of thin-walled concrete filled box columns, In: Proceedings International Conference on Composite Construction - Conventional and Innovative, Innsbruck, pp. 801–806, 1997.
101. Guo L. and Zhang S. (2007). Behavior of concrete-filled RHS steel tubes subjected to axial compression combined with bi-axial bending moment, In: Proceedings of the 3rd International Conference on Steel and Composite Structures (ICSCS07), Taylor & Francis, Manchester, UK., 2007
102. Tao Z, Han LH and Wang DY. (2007). Experimental behaviour of concrete-filled stiffened thin-walled steel tubular columns, Thin-Walled Structures, Vol. 45, no. 5, pp. 517–527
103. Hernández-Figueirido D, Romero ML, Bonet JL, and Montalvá JM. (2012a). Influence of Slenderness on High-Strength Rectangular Concrete-Filled Tubular Columns with Axial Load and Nonconstant Bending Moment, Journal of Structural Engineering, vol. 138, no. 12, pp. 1436–1445
104. Hernández-Figueirido D, Romero ML, Bonet JL, and Montalvá JM. (2012b). Ultimate capacity of rectangular concrete-filled steel tubular columns under unequal load eccentricities. Journal of Constructional Steel Research, Vol. 68, no. 1, pp. 107–117

105. Du Y, Chen Z, Wang YB, Liew JR. (2017). Ultimate resistance behavior of rectangular concrete-filled tubular beam-columns made of high-strength steel, Journal of Constructional Steel Research, Vol. 133, pp. 418-433.
106. Armaghani, D. J., Hajihassani, M., Sohaei, H., Mohamad, E. T., Marto, A., Motaghedi, H., & Moghaddam, M. R. (2015). Neuro-fuzzy technique to predict air-overpressure induced by blasting. Arabian Journal of Geosciences, 8(12), 10937-10950.
107. Momeni, E., Nazir, R., Armaghani, D. J., & Maizir, H. (2015). Application of artificial neural network for predicting shaft and tip resistances of concrete piles. Earth Sciences Research Journal, 19(1), 85-93.
108. Khandelwal, M., Armaghani, D. J., Faradonbeh, R. S., Ranjith, P. G., & Ghoraba, S. (2016). A new model based on gene expression programming to estimate air flow in a single rock joint. Environmental Earth Sciences, 75(9), 739.
109. Taormina, R.; Chau, K.; Sethi, R. Artificial neural network simulation of hourly groundwater levels in a coastal aquifer system of the Venice lagoon. Engineering Applications of Artificial Intelligence 2012, 25, 1670–1676, doi:10.1016/j.engappai.2012.02.009.
110. Thanh Duong, H.; Chi Phan, H.; Le, T.-T.; Duc Bui, N. Optimization design of rectangular concrete-filled steel tube short columns with Balancing Composite Motion Optimization and data-driven model. Structures 2020, 28, 757–765, doi:10.1016/j.istruc.2020.09.013.
111. Le, T.-T. Practical machine learning-based prediction model for axial capacity of square CFST columns. Mechanics of Advanced Materials and Structures 2020, 0, 1–16, doi:10.1080/15376494.2020.1839608.
112. Ali, F.; McKinney, J. Artificial Neural Networks for the Spalling Classification & Failure Prediction Times of High Strength Concrete Columns. Fire Engineering 2014, 5, 203–214, doi:10.1260/2040-2317.5.3.203.
113. Asteris, P.G.; Mokos, V.G. Concrete compressive strength using artificial neural networks. Neural Comput & Applic 2019, doi:10.1007/s00521-019-04663-2.
114. Hasanzadehshooiili, H.; Lakirouhani, A.; Šapalas, A. Neural network prediction of buckling load of steel arch-shells. Archives of Civil and Mechanical Engineering 2012, 12, 477–484, doi:10.1016/j.acme.2012.07.005.
115. Nguyen, H.Q.; Ly, H.-B.; Tran, V.Q.; Nguyen, T.-A.; Le, T.-T.; Pham, B.T. Optimization of Artificial Intelligence System by Evolutionary Algorithm for Prediction of Axial Capacity of Rectangular Concrete Filled Steel Tubes under Compression. Materials 2020, 13, 1205, doi:10.3390/ma13051205.
116. Asteris, P.G.; Armaghani, D.J.; Hatzigeorgiou, G.D.; Karayannis, C.G.; Pilakoutas, K. Predicting the shear strength of reinforced concrete beams using Artificial Neural Networks. Computers and Concrete 2019, 24, 469–488, doi:10.12989/cac.2019.24.5.469.
117. Psyllaki, P., Stamatiou, K., Iliadis, I., Mourlas, A., Asteris, P., Vaxevanidis, N. (2018). Surface treatment of tool steels against galling failure, MATEC Web of Conferences, 188, 04024.
118. Asteris, P.G., Argyropoulos, I., Cavaleri, L., Rodrigues, H., Varum, H., Thomas, J.,

Lourenço, P.B. Masonry Compressive Strength Prediction using Artificial Neural Networks. In International Conference on Transdisciplinary Multispectral Modeling and Cooperation for the Preservation of Cultural Heritage; Springer: Cham, Switzerland, 2018; pp. 200–224.

119. Apostolopoulou, M., Douvika, M.G., Kanellopoulos, I.N., Moropoulou, A., Asteris, P.G. (2018) Prediction of Compressive Strength of Mortars using Artificial Neural Networks. In: Proceedings of the 1st International Conference TMM_CH Transdisciplinary Multispectral Modelling and Cooperation for the Preservation of Cultural Heritage, 10-13 October, 2018, Athens, Greece
120. Nguyen, Q.H.; Ly, H.-B.; Tran, V.Q.; Nguyen, T.-A.; Phan, V.-H.; Le, T.-T.; Pham, B.T. A Novel Hybrid Model Based on a Feedforward Neural Network and One Step Secant Algorithm for Prediction of Load-Bearing Capacity of Rectangular Concrete-Filled Steel Tube Columns. Molecules 2020, 25, 3486, doi:10.3390/molecules25153486.
121. Le, T.-T. Prediction of tensile strength of polymer carbon nanotube composites using practical machine learning method: Journal of Composite Materials 2020, doi:10.1177/0021998320953540.
122. Asteris, P.G.; Roussis, P.C.; Douvika, M.G. Feed-Forward Neural Network Prediction of the Mechanical Properties of Sandcrete Materials. Sensors 2017, 17, 1344, doi:10.3390/s17061344.
123. Asteris, P.G.; Nikoo, M. Artificial bee colony-based neural network for the prediction of the fundamental period of infilled frame structures. Neural Comput & Applic 2019, doi:10.1007/s00521-018-03965-1.
124. Pham, B.T.; Nguyen-Thoi, T.; Ly, H.-B.; Nguyen, M.D.; Al-Ansari, N.; Tran, V.-Q.; Le, T.-T. Extreme Learning Machine Based Prediction of Soil Shear Strength: A Sensitivity Analysis Using Monte Carlo Simulations and Feature Backward Elimination. Sustainability 2020, 12, 2339, doi:10.3390/su12062339.
125. Ly, H.-B.; Pham, B.T.; Le, L.M.; Le, T.-T.; Le, V.M.; Asteris, P.G. Estimation of axial load-carrying capacity of concrete-filled steel tubes using surrogate models. Neural Comput & Applic 2020, doi:10.1007/s00521-020-05214-w.
126. Le, T.-T. Surrogate Neural Network Model for Prediction of Load-Bearing Capacity of CFSS Members Considering Loading Eccentricity. Applied Sciences 2020, 10, 3452, doi:10.3390/app10103452.
127. Asteris, P.G., Skentou, A.D., Bardhan, A., Samui, P., Pilakoutas, K. Predicting concrete compressive strength using hybrid ensembling of surrogate machine learning models, Cement and Concrete Research,2021, 145, 2021, https://doi.org/10.1016/j.cemconres.2021.106449.
128. Asteris, P.G., Cavaleri, L., Ly, HB. et al. Surrogate models for the compressive strength mapping of cement mortar materials. Soft Comput 25, 6347–6372 (2021). https://doi.org/10.1007/s00500-021-05626-3.
129. Armaghani, D.J., Asteris, P.G. A comparative study of ANN and ANFIS models for the prediction of cement-based mortar materials compressive strength. Neural Comput & Applic (2020). https://doi.org/10.1007/s00521-020-05244-4.
130. Lu, S.; Koopialipoor, M.; Asteris, P.G.; Bahri, M.; Armaghani, D.J. A Novel Feature

Selection Approach Based on Tree Models for Evaluating the Punching Shear Capacity of Steel Fiber-Reinforced Concrete Flat Slabs. Materials 2020, 13, 3902. https://doi.org/10.3390/ma13173902.

131. Apostolopoulou, M., Asteris, P.G., Armaghani, D.J., Douvika, M.G., Lourenço, P.B., Cavaleri, L., Bakolas, A., Moropoulou,A. Mapping and holistic design of natural hydraulic lime mortars,Cement and Concrete Research, 2020, 136, 106167, https://doi.org/10.1016/j.cemconres.2020.106167.
132. Armaghani, D.J., Hatzigeorgiou, G.D., Karamani, Ch., Skentou, A., Zoumpoulaki, I., Asteris, P.G. (2019). Soft computing-based techniques for concrete beams shear strength, Procedia Structural Integrity 17 (2019) 924–933.